TÉCNICO LISBOA

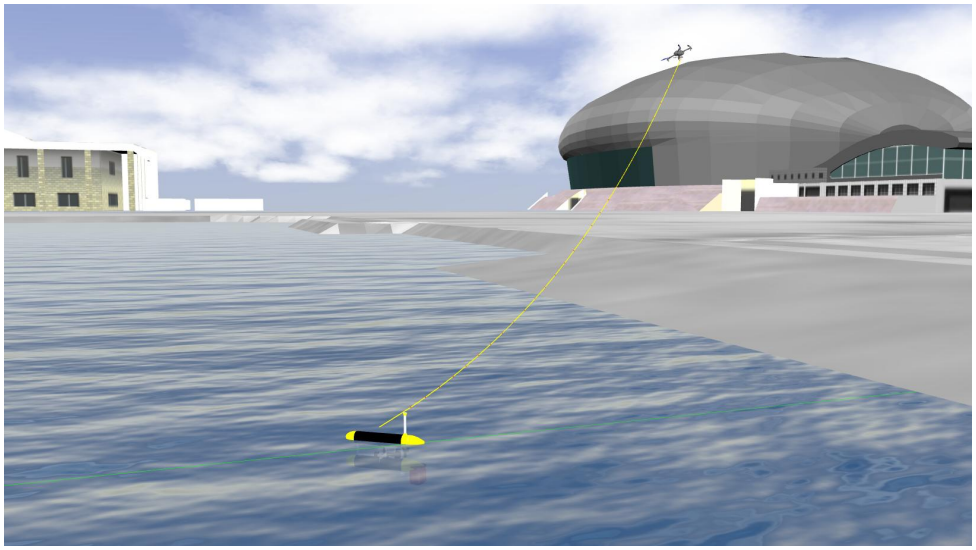

Cooperative Path-Following Control of Aerial and Marine Vehicles

António Manuel Fernandes de Sousa Antunes

Thesis to obtain the Master of Science Degree in

Electrical and Computer Engineering

Supervisors: Prof. Rita Maria Mendes de Almeida Correia da Cunha
Prof. António Manuel dos Santos Pascoal

Examination Committee

Chairperson: Prof. João Manuel de Freitas Xavier
Supervisor: Prof. Rita Maria Mendes de Almeida Correia da Cunha
Member of the Committee: Prof. David Alexandre Cabecinhas

December 2022

Declaration

I declare that this document is an original work of my own authorship and that it fulfills all the requirements of the Code of Conduct and Good Practices of the Universidade de Lisboa.

Acknowledgments

This master's dissertation is the culmination of 17 years of continuous learning and growth both as a student and as a man. So my recognition and gratitude go to all the people who were part of this journey, I am a little bit of all of them: those who challenged me, those who criticized me, those who made me smile, those who made me cry, those who made me better every day. To my teachers and colleagues, to my friends, to my Inês. And above all, to my parents, Fernando and Conceição, and sister, Catarina, who was always there from day one.

I thank Instituto Superior Técnico for the demand and excellence, the concepts, the culture and the vision, these are values that will certainly accompany me for my next chapters. But I am also grateful for the students, my colleagues, some of whom I take as friends for life. We were always together, in good times and in bad, as a team. To Francisco Velez, to João Paixão, to João Rosa, to Miguel Antunes, to Pedro Salgueiro.

I also must thank the people who contributed directly to this work. First of all, I have to thank Professor António Pascoal and Professor Rita Cunha for agreeing to work with me. Especially to Professor Rita Cunha for continuously guiding and helping me in this task, with all her patience and wisdom. It is essential to thank Marcelo Jacinto both for his collaboration and for his immeasurable helpfulness and willingness to help. This work was partially funded by Fundação para a Ciência e Tecnologia within the scope of the project (1018P.05390.1.01) EMSO-PT - PINFRA/22157/2016_LISBOA-01-01.

Abstract

This master's dissertation deals with a cooperative mission between an aerial and a marine vehicle connected by a tether. The tether is modelled as a cable with two suspension points and the corresponding equilibrium condition is studied. Subsequently, an analysis is made regarding the management of the cable length in order to allow the success of the mission, minimizing its impact on the vehicles and on the cable itself. This analysis converges to a function capable of computing the ideal length for the cable depending on the relative position of the vehicles. Next, to pave the way for the development of cooperation while following paths, models for the two types of vehicles are presented, as well as methods of controlling them. For the aerial vehicle, a hierarchical structure is adopted with an inner loop to control the orientation and an outer loop to control the translation movement. As far as the marine vehicle is concerned, two inner loops are used for the surge speed and the yaw rate. The Cooperative Path-following (CPF) is achieved through the use of a virtual target, as a facilitator of references for each vehicle. These targets are coordinated by a continuous synchronization protocol. Finally, results are presented in the form of simulations, first of each vehicle individually and then of both in formation interconnected by the cable. A plug-in is also introduced, in the context of a mission in Robot Operating System (ROS), created to incorporate a simulated cable in the *Gazebo* simulator.

Keywords

Unmanned Aerial Vehicle, Autonomous Surface Vehicle, Tether, Cooperative Path-following.

Resumo

Esta dissertação de mestrado aborda o desenvolvimento de uma missão cooperativa entre um veículo aéreo e um marinho ligados por um cabo. É apresentado um modelo de equilíbrio para o cabo suspenso entre o veículo aéreo e o veículo marinho de superfície. Posteriormente é feita uma análise referente à gestão do comprimento do cabo de modo a permitir o sucesso da missão minimizando o seu impacto nos intervenientes. Esta análise converge numa função capaz de indicar qual o comprimento ideal para o cabo dependendo da posição relativa dos veículos. Seguidamente, de modo a abrir o caminho para o desenvolvimento dos mecanismos de cooperação para o seguimento de caminhos, são apresentados modelos para os dois tipos de veículos bem como métodos de controlo destes. Para o veículo aéreo é adotada uma estrutura hierárquica com um ciclo interno para o controlo da orientação e um ciclo externo para o controlo referente ao movimento de translação. No que concerne ao veículo marinho são utilizados dois ciclos internos para a velocidade de avanço e para a velocidade de guinada. O seguimento de caminhos cooperativo é atingido através da utilização de um alvo virtual, como facilitador de referências para cada veículo. Estes alvos são coordenados por um protocolo de sincronização de caráter contínuo. Por último são apresentados resultados sob a forma de simulações, primeiramente de cada veículo a título individual e de seguida de ambos em formação interligados pelo cabo. É ainda introduzido um plug-in criado com vista à simulação do cabo no simulador *Gazebo*.

Palavras Chave

Veículo Aéreo não Tripulado, Veículo de Superfície Autónomo, Cabo, Seguimento de Caminhos Cooperativo.

Contents

List of Figures

List of Tables

Acronyms

ADRC	Active Disturbance Rejection Control
AHRS	Attitude and Heading Reference System
ASV	Autonomous Surface Vehicle
AUV	Autonomous Underwater Vehicle
CAD	Computer Aided Design
CPF	Cooperative Path-following
DOF	Degrees of freedom
DGPS	Differential Global Positioning System
DSOR	Dynamical Systems and Ocean Robotics Laboratory
DVL	Doppler Velocity Log
ETC	Event-Triggered Communications
GPS	Global Positioning System
IMU	Inertial Measurement Unit
ISR	Institute for Systems and Robotics
IST	Instituto Superior Técnico
LARSyS	Laboratory for Robotics and Engineering Systems
LOS	Line-of-sight
MAS	Multi-Agent Systems
NED	North-East-Down
PF	Path-following
PI	Proportional Integral
PID	Proportional Integral Derivative

ROS	Robot Operating System
SNAME	Society of Naval Architects & Marine Engineers
TT	Trajectory Tracking
3D	three-dimensional
3DR	3D Robotics
2D	two-dimensional
UAV	Unmanned Aerial Vehicle

1

Introduction

Contents

1.1 Motivation and Problem Definition

This Master's thesis addresses the problem of "Cooperative Path-Following Control of Aerial and Marine Vehicles". More specifically, the work is focused on studying cooperative scenarios where an unmanned aerial vehicle Unmanned Aerial Vehicle (UAV) and an autonomous surface vehicle Autonomous Surface Vehicle (ASV) are linked by a tether.

The cooperation between vehicles in certain environments can be a great way of increasing the performance and success rate of any mission. It also allows for the execution of more complex missions, for example, tasks that require two agents in two different locations at the same time. However, there is a big differentiating factor between both vehicles, which is autonomy. The aerial vehicles, electric multirotors, have typically an autonomy below 30 minutes, which can be extended or reduced depending on the kind of effort required by its flow of actions. The limited flight time can be disappointing if the goal is to perform longer missions or power-demanding tasks. The proposed solution, as previously stated, is the use of a tether as a power supply linking the two vehicles. The use of this type of link also provides a line of communication between the two agents. There is no need to attach data storage systems to the aerial vehicle, reducing its weight which will naturally lead to a potential improvement in performance. There are already some offers of tethered drones in the market for example Elistair [8], Hoverfly [9] and Viper Drones [10]. An example of a tethered drone connected to a fixed ground base station is presented in figure 1.1. Nonetheless, these offers tend to be for static situations such as live detection of natural disasters, subsequent monitoring and possible humanitarian support, road traffic control, increase of the range of telecommunication networks, video surveillance systems for example with the purpose of security of private property or even for crowd control, image collection and data acquisition, the list goes on.

Figure 1.1: Elistair tethered drone.

The goal is to offer the same possibilities but in a dynamic mode, instead of being fixed to a ground base station. In this mode, new possibilities emerge, for example, the surveillance and the detection of natural disasters can now be done by a single itinerant aircraft instead of a formation of fixed location ones. Another example integrated into the maritime context is the coastal patrol, which with a system of this kind can monitor a much larger area without an autonomy constraint. There is a condition for this approach to be effective, which has to do with the clearance of the environment in question: there is no room for obstacles that hinder the existence of the cable that connects the two agents. Another limitation is the length of the tether which can reduce the range of action of the drone. In academic terms, this approach is interesting from a control point of view because it is necessary to frame two completely different entities in terms of their dynamics and characteristics and design a controller capable of following a path while, at the same time, knowing how to deal with the disturbance caused by the cable in the aerial vehicle.

1.2 State of the art

The dynamics of UAVs and ASVs are widely studied and known. However, there are topics of study that still pose significant challenges, namely those related to cooperative control, tether modelling and handling, disturbance rejection and the reason why Path-following (PF) is chosen as opposed to Trajectory Tracking (TT). This chapter presents a brief literature review and contextualization regarding the state of the art of the topics in question.

1.2.1 Trajectory tracking vs Path-following

When one wants some vehicle to move from a certain point to another there are at least two ways to look at the way its movement is predefined, which are a trajectory or a path. A trajectory is a sequence of positions parameterized in time, which means that each point has an intrinsic intended velocity and acceleration. On the other hand, a path is a less restrictive approach, it defines only positions that must be followed by the vehicle and it might include a range of desired velocities.

For fully actuated systems there are plenty of acceptable nonlinear control solutions to track a trajectory that are very well known, as presented in [11]. However, for underactuated systems, like the quadrotor and the ASV, the problem is not so straightforward and some interesting techniques are still in study related to linearization and feedback linearization. These methods are built around working zones, so whenever the system encounters situations outside these zones, that is, on non-linear terrain, performance can eventually be compromised which means that the system can become unstable. Lyapunov control-based laws can be a solution to partially overcome this problem as explained in [12]. TT by being so time stringent can be too demanding by forcing aggressive maneuvers which cannot be performed

by some vehicles, for example, if saturation is achieved by the control signals. Usually, UAVs tend to be capable enough to do those aggressive moves however ASVs may not be able to complete the same task, it depends if the intended trajectory is slow and smooth enough for the ASV.

As described in [11] and [12], following a path devoid of time constraints is equivalent to tracking a speed profile while controlling the vehicle orientation to keep it within the path. The PF allows the vehicle to converge to the intended locations in a much smoother way when compared to the TT situation, avoiding saturation and therefore unfeasible actions. In [13] there are many suggested methods to solve this problem such as Backstepping, Lyapunov control-based, Feedback Linearization control-oriented algorithm and, of geometric character, Carrot-chasing type. The ASVs are an example of a class of vehicles that are less capable of reproducing aggressive maneuvers, therefore path following is recommended instead of TT. The fact that the main objective is to cooperatively control both a UAV and a ASV makes it understandable to choose the PF method since a trajectory-tracking strategy could be too demanding for the ASV limitations. The chosen strategy which is further explored in Chapter 5 is the use of a virtual target as a Carrot-chasing type of PF strategy.

1.2.2 Path-following Strategies

As previously said there are plenty PF possible approaches, for example in [14] it is proposed for ASVs a guidance law based on Line-of-sight (LOS) which is one of the most basic algorithms used. This kind of algorithm achieves PF by always steering to a point that is ahead of the vehicle's current projection in the path under a predefined speed profile. The distance between the projection and the reference is a fixed value.

In [1] the authors first introduce algorithms that allows to follow either a straight line or a circular orbit by steering along with a vector field that points onto the path, which one can easily set as being more or less aggressive. Then it moves on to expand it as two different PF techniques based on the assumption that any two-way points can be connected by straight lines and orbits. The first strategy prioritizes that the vehicle passes as close as possible to each waypoint, neglecting the path described between each of those. In this strategy, the path between two waypoints is always a straight line and the vehicle only starts following the next straight line when it goes through the orthogonal plane to both stretches of the path. The second strategy prioritizes following the intended path more than getting the closest to each waypoint. This is achieved by introducing a fillet, which is an arc of circumference, in the transition between the straight line that connects two pairs of waypoints. Representations of paths described by a vehicle using each one of these strategies are shown in figure 1.2.

Another approach is presented in [15] which defines a more balanced solution for the PF problem with the help of a virtual target that dynamically updates itself depending on the current state of the vehicle. It is defined two control laws, one for the virtual target and another for the references which are

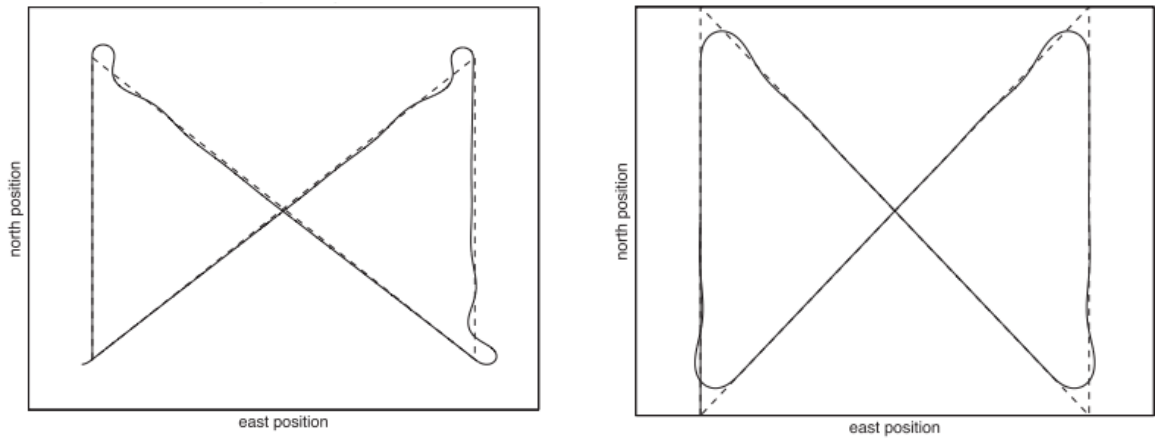

(a) Waypoints connect by straight lines.

(b) Waypoints connect by straight lines and fillets.

Figure 1.2: Two path-following strategies that prioritize either the closeness to each waypoint or to the whole shape of the path (adopted from [1]).

to be followed by the vehicle. This option gives a lot of freedom for the designer to ask for smoother or more aggressive maneuvers depending on what is desired or on which vehicles are being used.

1.2.3 Cooperative Path Following

The idea of controlling a vehicle while dealing with constraints related to its own or even to the environment and its uncertainty can be challenging, however, it becomes much more when one needs to control a group of several agents, coordinated and eventually with different input constraints. When designing such a system one has to take into account factors like the topology of the communication between vehicles, its cost and even the fact that the flow of information between the agents may be discrete and suffer some delays and losses.

In [16] and in [17] it is mentioned that the typical strategy to solve the Cooperative Path-following (CPF) problem is to split the problem into two subproblems. The first step is to control individually each vehicle to follow a virtual target by steering in convergence to it and therefore to the desired path with an assigned speed. The second step is to control all target speeds to get coordination and keep the formation pattern.

In [16] is also pointed to one of the main problems of cooperative control: communication, the authors derive a CPF algorithm that includes logic-based communication in order to reduce it to the strictly necessary scenarios. To do so the vehicles can only communicate with some of the closest ones of the formation, which may help to mitigate both delays and losses. The proposal is to design decentralized controllers that use their state and the states of those agents estimated locally. The communication only occurs when the error between the state and its estimate locally exceeds a predefined threshold.

With the same goal of reducing the frequency of communications in [18] and in [19] a distributed control strategy is presented with an event-triggered communication mechanism as a solution for the problem of consensus/synchronisation for networked nonlinear Multi-Agent Systems (MAS). In [20] consensus is defined as "to reach an agreement regarding a certain quantity of interest that depends on the state of all agents" and a consensus algorithm as "an interaction rule that specifies the information exchange between an agent and all of its neighbours on the network". The authors present to the reader the theoretical-practical aspects of the problem of consensus, whose approaches are influenced by graph theory. As said before this problem is very relevant in the context of cooperative control of a MAS, which is covered in [21].

As it is going to be further explored in the following chapters the usage of a tethered connection between vehicles solves the problem of communication, a cable creates a continuous communication scenario, at least as continuous as it can be, with very little cost in terms of energy when compared to other methods of non-wired distant transmissions.

1.2.4 Disturbance Rejection

Disturbances must be taken into account when one wants to control any vehicle, at least if one wants to get it to the real world. If we are talking about UAVs, the wind is the most important disturbance to be aware of while if we talk about ASVs, it is the ocean currents we want to look at. The classical approach of control theory to deal with this class of problems is a Proportional Integral Derivative (PID) controller, whose integral part has the effect of rejecting constant perturbations.

In the past few decades efforts have been made with the purpose of solving this problem via new methods based on modern control. For example, in [22] is proposed the Active Disturbance Rejection Control (ADRC) that merges the error-based approach of control with the state observer. The authors point out that this ADRC strategy is subdivided into a transient trajectory generator, nonlinear feedback combination and the estimation of disturbance and its rejection.

On the other hand, there have been also ideas regarding backstepping in order to solve this problem. Backstepping is a recursive technique that allows the design of a Lyapunov-based feedback controller that ensures global asymptotic stability for strict feedback systems, which means that are only dependent on their states. As highlighted in [23], normally this method is not applicable in underactuated systems, however, the fact that the models used are feedback linearizable makes it possible to be stabilized by the backstepping method. The authors present a nonlinear adaptive state feedback controller based on adaptive backstepping which uses an estimator as a tool to get the desired disturbance rejection. This adaptive strategy gives the system the desired robustness against external constant disturbances such as constant wind.

1.2.5 Tether Model and Rejection

In addition to the disturbances already mentioned, there is also the one caused by the tether. In [24] a solution to a TT problem is presented in which a UAV is connected to a moving platform by means of a tether in tension that passively varies its length through a winch, which applies a non-controllable constant torque.

In this project, the link will not be fully stretched. It should also be noted that only the impact of the cable on the aerial vehicle is considered since its effect on the ASV is residual. In sum, it is adequate to state that the tether is a constant disturbance over the UAV. This scenario is related to UAV slung load transportation. This problem can be solved for example via Lyapunov control laws and backstepping techniques, the same treatment as any other disturbance, as it is presented in [25] and in [26].

The idea is to have a tether that is loose or collected depending on some conditions: to avoid contact with water, to keep the cable away from being fully stretched and also to have some heave tolerance regarding the sea waves. This would be done by a winch similar to the one described in [2].

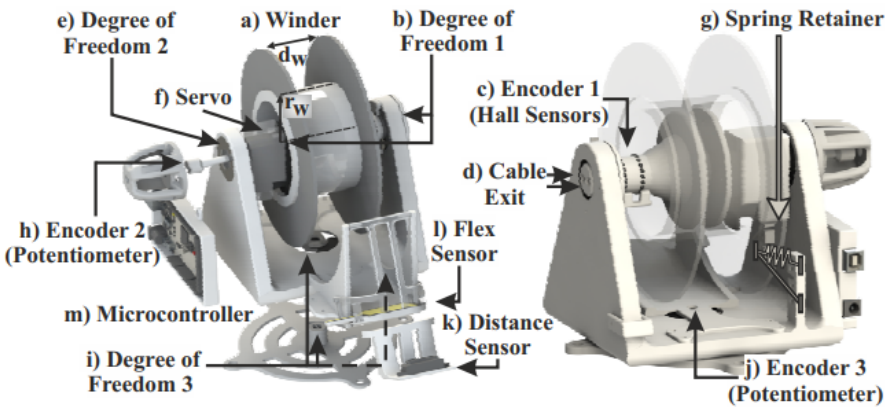

Figure 1.3: Detailed designed of a smart winch (adopted from [2]).

In [27] and [28] the modelling of this cable is done by adapting the case of a catenary hanging on two points in space, always aware of all the physical involvement with regard to aerodynamics and other forces. In [29] and [3] it is done a similar analysis regarding the tether model and also a discrete model that relates some categories of desired tether configurations and the relative position between the ASV and the UAV, this approach is further studied and developed in Chapter 2.

1.3 Thesis Outline

Besides the current Introduction chapter where the motivation for this topic is explored, the current state of the art regarding its related issues and how will this thesis contribute to that, there are also another

six chapters,

- **Chapter 2 - Tether - Modelling and Dynamic Operation**: presents an analysis of the kinematics and dynamics of a cable that is hanging on two separate points in space, describing a catenary, and then also studies the flying space of a UAV with a tether attached to an ASV and how to keep the tether within its desired behaviour.
- **Chapter 3 - Unmanned Aerial Vehicle (UAV) - Modelling and Control**: introduces the kinematics and dynamics of a quadrotor and then an inner-loop outer-loop control structure with the ability to reject disturbances, including the tether.
- **Chapter 4 - Autonomous Surface Vehicle (ASV) - Modelling and Control**: introduces the general kinematics and dynamics of a marine vehicle which are then simplified for the specific surface case; Then two control laws are defined, one for the surge speed and another for the yaw-rate.
- **Chapter 5 - Cooperative Path-following (CPF)**: firstly it is defined PF strategies for each vehicle, then it is adopted a unified approach that merges everything into a single cooperative system.
- **Chapter 6 - Cooperative System Simulation**: simulations of individual missions are presented for each vehicle that then converges to a joint mission of the two vehicles connected by a tether. A plug-in is also introduced to simulate tether in *Gazebo* also in a cooperative mission context.
- **Chapter 7 - Conclusion and Future Work**: the work carried out in this master's thesis is recapitulated and the possible next steps are suggested.

1.4 Main Contributions

The contributions regarding the work developed for this thesis are

- The study and modelling the tether as a catenary and the presentation of strategies to deal with the constraints that shall arise in such a cooperative mission.
- The study and description of dynamic models for aerial and marine vehicles, such as the quadrotor and a surface marine vehicle.
- The critical analysis of several PF strategies as well as cooperation techniques.
- Implementation and simulation of all the studied topics as a whole system.
- Development of a *Gazebo* plug-in that allows simulation of a dynamic tether, with changing length, linking an UAV and an ASV in a *ROS* environment developed in Dynamical Systems and Ocean Robotics Laboratory (DSOR) in Institute for Systems and Robotics (ISR).

2

Tether - Modelling and Dynamic Operation

Contents

2.1 Tether Model

As specified before the system in study is a cooperative team of two vehicles, an Autonomous Surface Vehicle (ASV) and a Unmanned Aerial Vehicle (UAV) connected by a tether. This tether has two mounting points, one on the downside of the aerial vehicle and another on the upside of the marine vehicle. The first point is a simple cable connection and the second one is a pulley able to roll and unroll the cable, autonomously as is going to be shown later in this chapter. This pulley might have some elevation from the water, which can create some margin to avoid touching the water. However, for water contact avoidance analysis during this chapter, only the worst-case scenario will be taken into account, the pulley is at the same height as the water. The main goal of this chapter is to pursue a strategy that keeps the tether from being taut or touching the water by using different lengths depending on the relative positions of the vehicles. An illustration of the desired system is presented in figure 2.1. The tether will be considered for lower height applications, below 1 km.

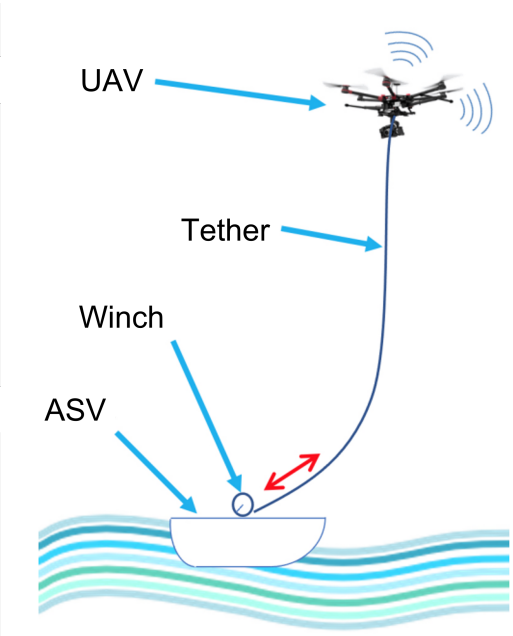

Figure 2.1: Representation of an UAV and an ASV linked by a tether. (adopted from [3]).

2.1.1 Tether Forces

There are three types of forces exerted on a tether in this scenario, a cooperative mission between an aerial and a marine surface vehicle linked by such a structure. Those forces are the cable's weight, the aerodynamic drag force and the tension forces caused by its interaction with the vehicles as presented in [28].

2.1.1.A Tether Weight

This is the main force, the one that might impact the most the system. It depends on the mass of the tether which is also dependent on two values, its linear weight density μ_t, which is the result of the product between the acceleration of gravity and the linear mass density of the tether, and its length,

$$w_t = \mu_t L_t \quad [N]. \tag{2.1}$$

The choice of the tether linear mass density is of the utmost importance and must take into account the ability of the UAV to reject the disturbance caused by the tether. A heavier tether requires more thrust to hold it and still has thrust to spare for all the tasks one desires to assign to the vehicle.

2.1.1.B Aerodynamic Drag

During a mission, while both vehicles are moving, the tether is subject to aerodynamic forces. There are two types of drag, the pressure drag which is perpendicular to the tether and represents most of the aerodynamic influence on this body, and the friction drag which is tangential to the tether. The friction drag is one order of magnitude below the pressure drag and usually gets a more important role in much bigger lengths than the ones desired for this project, therefore its impact can be neglected when one wants to model this system.

The aerodynamic drag force is computed as,

$$F_{D_t} = q_t C_{D_t} d_t L_t \quad [N], \tag{2.2}$$

where the C_{D_t} is the tether pressure drag coefficient, d_t is the diameter of the cross-section of the tether, and q_t is defined as,

$$q_t = \frac{1}{2}\rho \bar{V_t}^2 \quad [Pa], \tag{2.3}$$

where ρ is the fluid density, in this case, the density of the air, and $\bar{V_t}$ is the average relative fluid velocity orthogonal to the tether. It is important to point out that the drag depends quadratically on the relative speed between the cable and the air, which means that its absolute value increases when the velocity of the tether increases or when the wind speed increases.

2.1.1.C Tether Tension

The movement of the vehicles may create tension forces in the tether, especially when it is fully stretched. This tension is limited by the thrust of the UAV, which is the maximum force it can output against the tether. This is a force effect one wants to avoid, it can be harmful to the system for example by increasing

the power consumption to reject such a disturbance. Later in this chapter, an analysis is made to choose an acceptable working zone, which can avoid such a demanding scenario for the system.

2.1.2 Tether Equilibrium

The tether behaviour can be described through several moments, the take-off, the flight in which both vehicles move across space simultaneously, waypoint tasks in which the ASV is in a fixed location and the UAV may move within its flight envelope to perform any kind of mission and landing. In all of these situations, the tether will be modelled in a fully-elevated state through quasi-static catenary equations as it is in [28]. A free-body diagram illustrating the system in study is in figure 2.2.

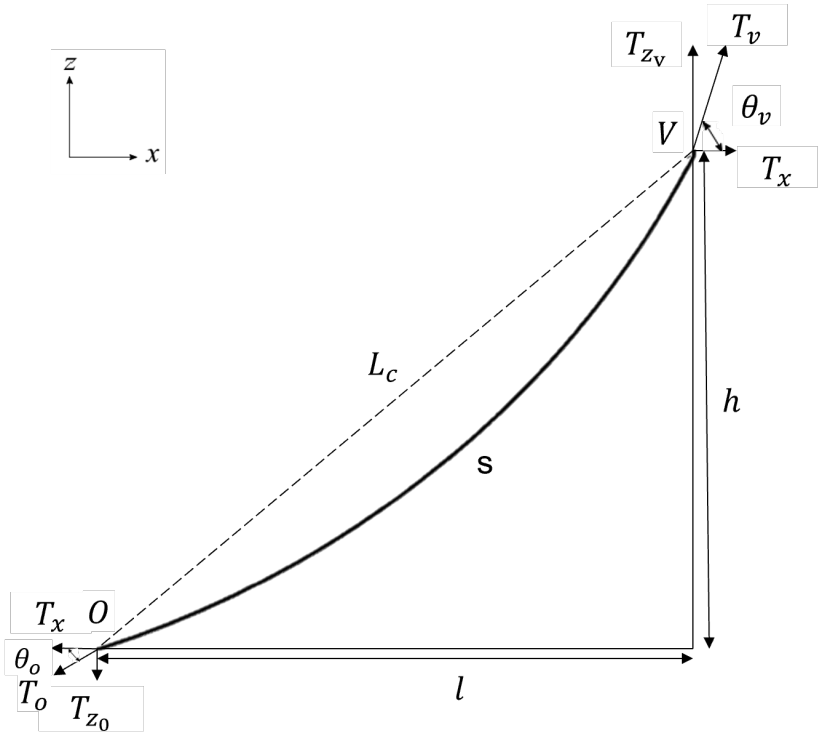

Figure 2.2: Free-body diagram illustrating a fully-elevated tether.

Assuming an equilibrium of forces the following is derived,

$$T_v(x - x_0)sin(\theta(x)) = \mu_t s(x - x_0), \tag{2.4}$$

$$T_v(x - x_0)cos(\theta(x)) = T_x, \tag{2.5}$$

$$tan(\theta(x)) = \frac{dz}{dx}. \tag{2.6}$$

By joining equations (2.5) and (2.6) into (2.4),

$$\frac{dz}{dx} = \frac{\mu_t}{T_x} s(x - x_0). \tag{2.7}$$

Also, it is important to clarify that the derivative of the arc-length is

$$\frac{ds}{dx} = \sqrt{1 + \left(\frac{dz}{dx}\right)^2} \tag{2.8}$$

Which makes it possible to define

$$\frac{d^2z}{dx^2} = \frac{\mu_t}{T_x}\frac{ds}{dx} = \frac{\mu_t}{T_x}\sqrt{1 + \left(\frac{dz}{dx}\right)^2}. \tag{2.9}$$

By integrating the equation (2.9) twice, a function of z in order to x is derived,

$$\frac{dz}{dx} = \sinh\left(\frac{\mu_t}{T_x}x + C_1\right), \tag{2.10}$$

$$z(x) = \frac{T_x}{\mu_t}\cosh\left(\frac{\mu_t}{T_x}x + C_1\right) + C_2. \tag{2.11}$$

In this situation, a tether describes a well-known shape: the catenary. The equation (2.11) is the catenary equation adapted to this problem. The constants C_1 and C_2 will allow the catenary to no longer be a generic shape but to be exactly where it is supposed to be between the two tether fixed extremities. Then the expressions for the values of both the mentioned constants and T_x will be determined, given the coordinates of the hanging points and the length of the cable. These two points are $(0, 0)$, considering the origin of the referential as the ASV connection to the tether, and (l, h) as the UAV connection to the tether.

By using the point $(0, 0)$ it is possible to get

$$C_2 = -\frac{T_x}{\mu_t}\cosh(C_1). \tag{2.12}$$

With the point (l, h) and with the equation (2.12) the other constant is derived,

$$h = \frac{T_x}{\mu_t}\cosh\left(\frac{\mu_t l}{T_x} + C_1\right) - \frac{T_x}{\mu_t}\cosh(C_1), \tag{2.13}$$

$$\frac{\mu_t h}{T_x} = 2\sinh\left(\frac{\frac{\mu_t l}{T_x} + C_1}{2}\right)\sinh\left(\frac{\mu_t l}{2T_x}\right), \tag{2.14}$$

$$C_1 = \sinh^{-1}\left(\frac{\mu_t h}{2T_x \sinh(\frac{\mu_t l}{2T_x})}\right) - \frac{\mu_t l}{2T_x}. \tag{2.15}$$

The angles of departure of the tether in both vehicles are given by joining equations (2.6) and (2.10),

$$\theta_O = tan^{-1}(\sinh(C_1)), \tag{2.16}$$

$$\theta_V = tan^{-1}\left(\sinh\left(\frac{\mu_t l}{T_x} + C_1\right)\right). \tag{2.17}$$

The vertical force exerted by the tether on each hanging point is

$$T_{z_O} = T_x tan\theta_O, \tag{2.18}$$

$$T_{z_V} = T_x tan\theta_V. \tag{2.19}$$

To compute the applied torque by the tether on the aircraft with

$$\tau_V = S(f)R^T T_V, \tag{2.20}$$

where R^T is the orientation of the axis of the body-fixed frame with respect to the body-fixed reference frame which is given by ${}^B_I R \in \mathbb{SO}(3)$ the transpose of (3.1), f is the mounting point of the tether on the UAV on its body-frame and $S(f)$ its respective skew-matrix

$$S(f) = \begin{bmatrix} 0 & -f_z & f_y \\ f_z & 0 & -f_x \\ -f_y & f_x & 0 \end{bmatrix}. \tag{2.21}$$

that allows computing the cross-product.

A function is to be defined to compute the horizontal reaction force T_x. It can be done by joining equations (2.8) and (2.10),

$$\frac{ds}{dx} = \sqrt{1 + \sinh^2\left(\frac{\mu_t}{T_x}x + C_1\right)} = \cosh\left(\frac{\mu_t}{T_x}x + C_1\right). \tag{2.22}$$

Integrating the equation (2.22) yields a function for the tether length from the mounting point in the ASV to any specified value for the horizontal component of the position,

$$s(x) = \frac{T_x}{\mu_t}\sinh\left(\frac{\mu_t}{T_x}x + C_1\right) + C_3. \tag{2.23}$$

Similarly to equation (2.12), the point (0,0) is used to get an expression for

$$C_3 = -\frac{T_x}{\mu_t}\sinh(C_1). \tag{2.24}$$

By using the UAV mounting point (l,L_t) which is the maximum horizontal displacement in reference

to the ASV mounting point where the tether length is maximum,

$$L_t = \sqrt{h^2 + \frac{4T_x^2}{\mu_t^2}\sinh^2\left(\frac{\mu_t l}{2T_x}\right)}, \tag{2.25}$$

this expression can be rewritten to ease the derivation in order to T_x,

$$\sqrt{L_t^2 - h^2} = \frac{2T_x}{\mu_t}\sinh\left(\frac{\mu_t l}{2T_x}\right), \tag{2.26}$$

therefore the function can be defined as

$$f_0 = \frac{2T_{x_n}}{\mu_t}\sinh\left(\frac{\mu_t l}{2T_{x_n}}\right) - \sqrt{L_t^2 - h^2}. \tag{2.27}$$

To compute the horizontal reaction force T_x a numerical method, the Newton Method is used since f_0 is a transcendental equation which cannot be turned into an algebraic one. The method consists of iteratively approximating the roots of a zero function f_0 and by doing that finding a good estimate for the horizontal force T_x. The method is described by

$$T_{x_{n+1}} = T_{x_n} - \frac{f_0}{\frac{\partial f_0}{\partial T_{x_n}}}. \tag{2.28}$$

To perform the method the partial derivative $\frac{\partial f_0}{\partial T_{x_n}}$ has to be computed as presented,

$$\frac{\partial f_0}{\partial T_{x_n}} = \frac{2}{\mu_t} sinh\left(\frac{\mu_t l}{2T_{x_n}}\right) - \frac{l}{T_{x_n}} cosh\left(\frac{\mu_t l}{2T_{x_n}}\right). \tag{2.29}$$

To increase the performance of this method, which is essential in a real scenario, an initial estimate T_{x_0} must be defined. To do so the Maclaurin series expansion of the hyperbolic sine was used up to the fifth power,

$$sinh(x) = x + \frac{x^3}{3!} + \frac{x^5}{5!} + ... \tag{2.30}$$

Using this expansion regarding f_0/l creates an expression in which the only variable is the T_{x_n} in $x = \frac{\mu_t l}{2T_{x_n}}$,

$$\frac{f_0}{l} = \frac{1}{x}\sinh(x) - \frac{\sqrt{L_t^2 - h^2}}{l} = 1 + \frac{x^2}{3!} + \frac{x^4}{5!} - \frac{\sqrt{L_t^2 - h^2}}{l}. \tag{2.31}$$

The expression (2.31) can be rewritten as a fourth-degree polynomial, which is a biquadratic equation,

$$ax^4 + bx^2 + c = 0 \tag{2.32}$$

in which the coefficients are

$$a = \frac{1}{120}, \tag{2.33}$$

$$b = \frac{1}{6}, \tag{2.34}$$

$$c = 1 - \frac{\sqrt{L_t^2 - h^2}}{l}. \tag{2.35}$$

Then by solving the biquadratic equation with the quadratic formula x^2 is found, which means that the initial estimate for T_{x_n} is available as

$$T_{x_0} = \frac{\mu_t l}{2x}. \tag{2.36}$$

2.1.3 Tether Dynamics

Despite being considered a quasi-static scenario to define the tether governing equations, in which it is always very close to equilibrium either in terms of shape or tension. One needs always to account for the dynamics which, especially in extreme scenarios, may lead to relevant disturbances in the tether and finally in the whole system.

In [28] the tether is seen as a string, whose possible disturbances are oscillatory in nature. There are two types of waves in a string, the longitudinal which acts tangentially to the tether and the transversal which are perpendicular to the tether. Those two types of waves may exist due to only two agents, aerodynamic forces and the UAV. Any disturbance that reaches the fundamental frequency or its harmonics can resonate and create a high-amplitude wave, that might be harmful to the system in particular for the UAV.

2.1.3.A Longitudinal Disturbances

The stiffness of the tether is much larger than the tension forces to which it is subjected, this means that its fundamental frequency is greater than the frequency of the excitation caused by the aircraft, avoiding the resonating effect. The aerodynamic longitudinal effect on the tether is not big enough to disrupt or deform the cable.

2.1.3.B Transversal Disturbances

Transversal waves may affect the tension both in the ASV and the UAV. This can be harmful to the aircraft since it is dealing over time with the tether disturbance. The transversal excitation of the tether may arise as one of two aeroelastic flutter types of occurrences, the conductor gallop and the vortex shedding.

The conductor gallop is an oscillatory high-amplitude but low-frequency (0.1 - 1 Hz) phenomenon found in cables subjected to wind, like the tether in study. It happens to non-symmetrical cables. This lack of symmetry is the reason why those cables are prone to this kind of effect, they are unstable in terms of aerodynamics. The obvious solution is to use a tether with a symmetric cross-section, a circular one may be the way to go.

Vortex shedding is an oscillatory low-amplitude but high-frequency phenomenon which is created by the flow of air passing through a body, this flow generates a low-pressure vortex in the back of the body which oscillates from side to side. This translates into an oscillation in the actual body. If the vortex oscillation frequency is equal to the fundamental frequency of the body, this body starts to resonate. However as presented in [28] the range of values of each frequency is separated, including the significant harmonics, thus they will not match each other.

In addition to the wind, the aircraft can also impact the cable. Vigorous radial position changes may create scenarios where the cable starts to oscillate, however, this oscillation tends to be less energetic than the initial movement and to vanish over time, thus not being harmful. However, if those changes are tangential it is possible for the UAV to make the tether resonate, in which case safety measures would be required, for example, the decoupling of the tether and the aerial vehicle.

2.2 Flying Space

To connect a tether between an ASV and an UAV in a marine scenario there are some constraints that one needs to take into account.

1. The tether must not get in the water. This means that if its departure point in the ASV, in the worst-case scenario, is barely at the water's level its departure angle has to be bigger or equal to zero degrees.

2. The distance between the UAV and the ASV must always be smaller or equal to the tether maximum length. In practice, the vehicles should operate within some distance from this borderline scenario. This is another event to account for when designing the safety measures mentioned above.

3. The tension exerted by the tether in the UAV must never surpass its maximum thrust. It is a good practice to have a margin between this maximum achievable tension and the maximum thrust of the vehicle. The aerial vehicle can be protected regarding this concern at an early stage of the implementation by selecting a tether whose weight is fully supported by the UAV with some thrust to spare. On the other hand, it is also good practice to prevent the cable from being fully stretched, it can lead to the UAV trying to move farther away with an increasingly bigger cost. Forcing against

the maximum length of the tether can ultimately lead to unnecessary spending of energy by the aerial vehicle or, in the worst-case scenario, breaking the link between the vehicles. This is very similar to what was mentioned in the previous topic which is dealt with safety measures.

A fully-elevated tether scenario is assumed, in which the cable is completely unrolled vertically during take-off and completely rolled during landing. To fulfil the points presented above there are very few relative positions between the vehicles in which the tether would behave as expected. Those positions are located near the maximum distance points, the hemispherical surface of radius equal to the fixed tether length. This is shown for a tether with a length of 50 m by the 2D discretization of the flying space present in figure 2.3.

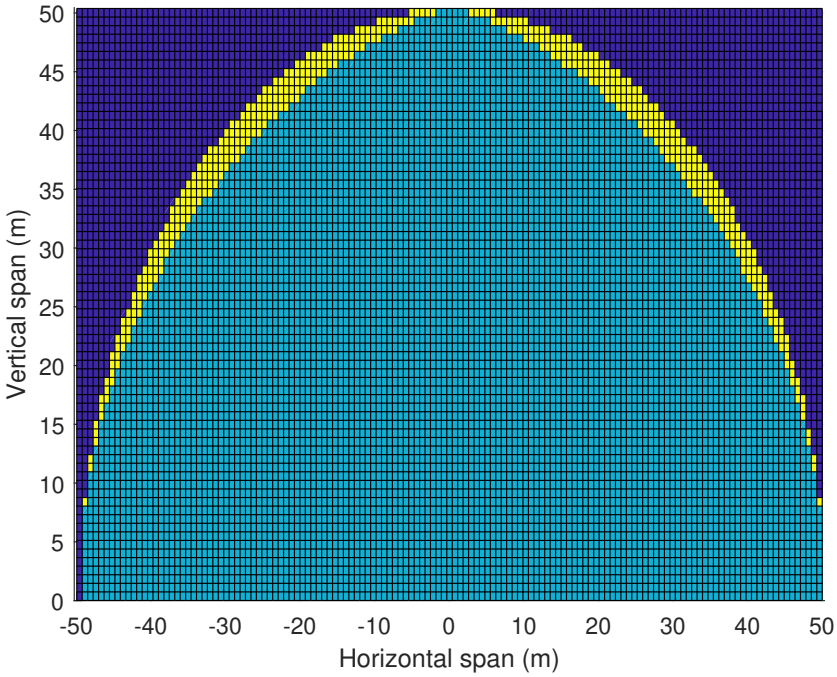

Figure 2.3: 2D discretization of the flying space. A position in yellow is a valid position. A position in light blue is invalid due to the tether's departure angle being smaller than zero which means that it contacts with the water. A darker blue position is out of the tether range.

A fixed tether length is quite restrictive for such a system. For some positions errors need to bem smaller than 1 m which might not be compatible with Global Positioning System (GPS). It reduces the margin for unforeseen events or systematic errors. For example, in a marine environment a vertical displacement, caused by the swell, of the mounting point of the tether in the ASV will easily bring the relative position of the two vehicles to the light blue zone of figure 2.3 which may lead to contact between the cable and the water.

That said, it became clear that the solution goes through a pulley system capable of varying the

length of the cable depending on the relative position of the vehicles.

2.3 Flying Space with a Dynamic Tether Length

This section presents an analysis of the desired working zone of the tether regarding its departure angle, its length and the tension exerted on the UAV. The approach is similar to the one in [29], however, adapted to the equilibrium described in previous sections as well as with other choices of values, for example, the value for μ_t is $0.294\,N\,m^{-1}$. For example purposes, the maximum tether length chosen in this section is also 50 m.

In order to better understand the desired shape for the tether for any relative position between vehicles, four notable catenaries represent limit scenarios. The maximum tether length catenary which is not desirable for this relative position is the worst-case scenario where contact with the water is a very probable outcome. The minimum tension catenary is still an undesirable configuration because the departure angle of the tether from the mounting point is negative, pointing downwards, which means that it is pointing downwards. The slack catenary represents the boundary between a valid shape and an invalid one. Finally, the taut catenary which is the fully stretched cable, its length is equal to the distance between the mounting point in the ASV and the UAV. Those four representations are presented in figure 2.4.

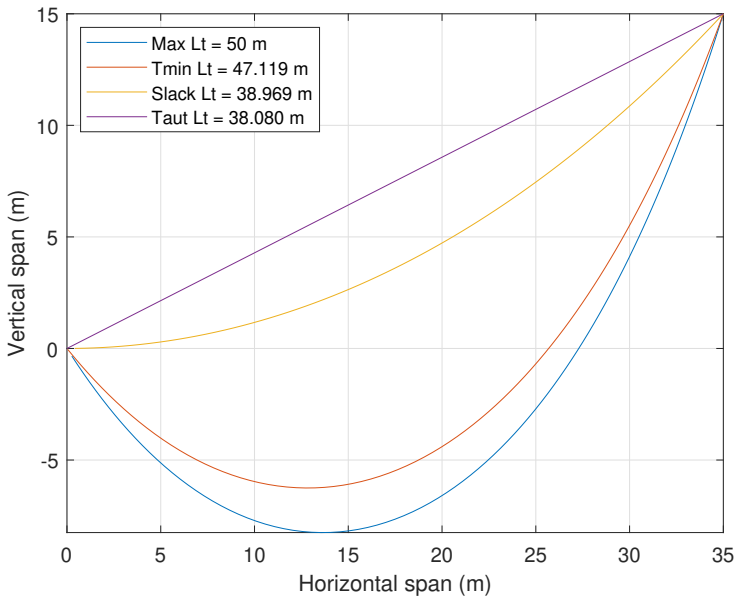

Figure 2.4: Notable catenaries for a relative position of $(l, h) = (35, 15)\,m$.

This figure allows the visualization of the desired working zone, between the slack and taut lengths. In that zone, the departure angle is always positive, pointing upwards, which is the ultimate goal. However

there are other factors to take into account, the tension exerted in the UAV should be as low as possible to reduce its disturbance effect and the power consumption. A representation for a fixed relative position $(l, h) = (35, 15)\, m$ the tension exerted by tether at the UAV as a function of the tether length is shown in figure 2.5.

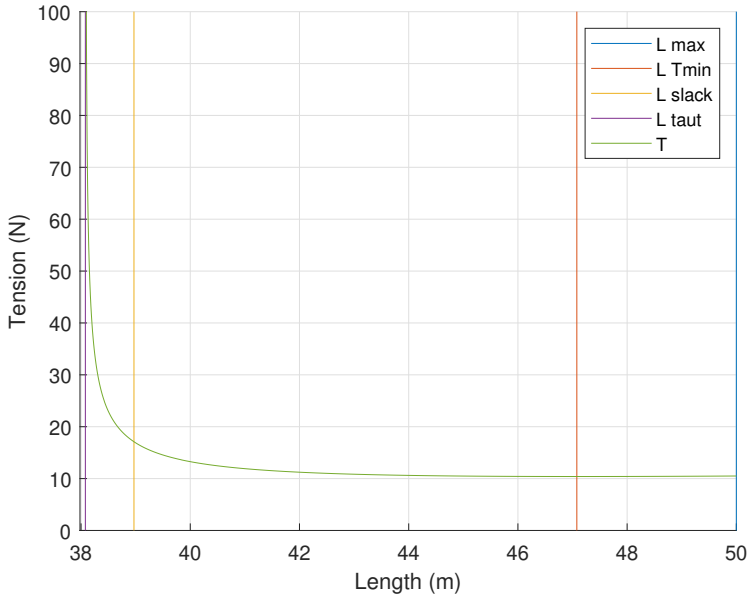

Figure 2.5: Tension exerted by the tether in the UAV as a function of the tether length. Notable points are also assigned, maximum length, minimum tension, slack and taut configurations.

Decreasing from the slack length to the taut length leads to increasing tension in the aerial vehicle. The growth rate gets asymptotically bigger, virtually to infinity which is not the reality, as the length tends to the taut length. In [29] it is suggested as viable options to seek lengths that increase the tension on the UAV by 5%, 10% and 20%. Each option can be better than one another depending on the system in question, maybe a system that deals with a heavier tether, either by its density or length, should use a length closer to the slack which would relieve the amount of tension the UAV is holding. If one is in a situation where the load on the UAV is less of a concern then one might want to opt for a bigger margin.

2.3.1 Polynomial Fit for a Tether Length Function

By re-discretizing, the two-dimensional (2D) space as it was done in 2.3 and computing for each position which length leads to minimum tension, slack, 5%, 10% or 20% increasing tension yields the following graphs in figure 2.6.

This figure is the result of the polynomial fit of 3^{rd} degree of the data computed for each point in the bi-dimensional space after being normalized through the relative height between vehicles. This approximation consists of finding the coefficients that better fit this expression,

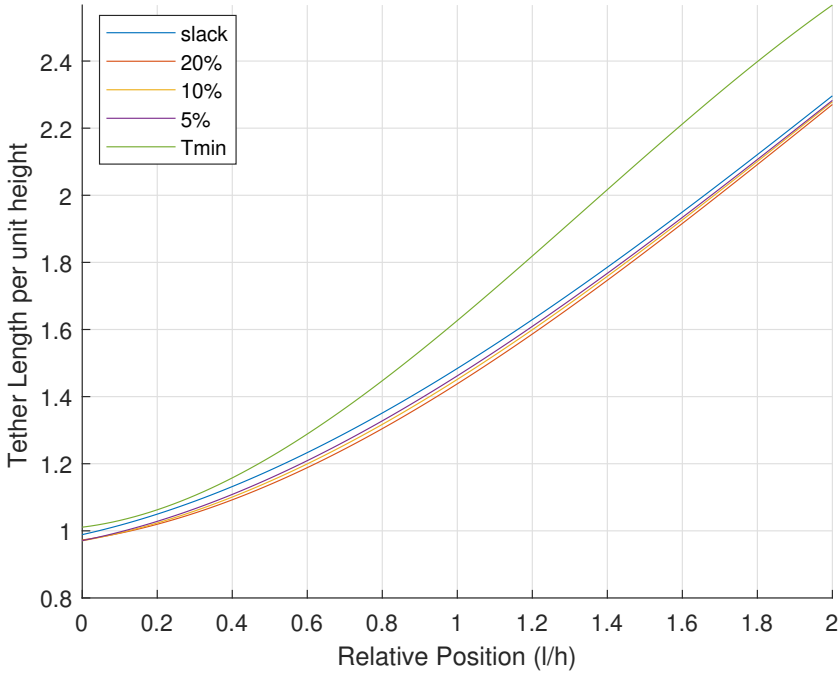

Figure 2.6: Polynomial fit of 3^{rd} degree for the length of the tether per unit height that leads to notable scenarios such as minimum tension, slack, 5%, 10% or 20% increasing tension depending on the relative position.

$$\frac{L_t}{h} = c_1 + c_2\frac{l}{h} + c_3\left(\frac{l}{h}\right)^2 + c_3\left(\frac{l}{h}\right)^3, \tag{2.37}$$

which can be easily transformed into the length as a function of the relative position by multiplying both members by the height,

$$L_t = c_1 h + c_2 l + c_3\frac{l^2}{h} + c_4\frac{l^3}{h^2}. \tag{2.38}$$

The table 2.1 has the coefficients and its R^2 corresponding to the confidence in the least squares approximation.

L	c_1	c_2	c_3	c_4	R^2
L_{Tmin}	1.0109	0.1385	0.6348	−0.1575	0.9663
L_{slack}	0.9887	0.2492	0.2898	−0.0437	0.9995
L_5	0.9708	0.2268	0.3142	−0.0498	0.9995
L_{10}	0.9703	0.2012	0.3331	−0.0533	0.9996
L_{20}	0.9727	0.1650	0.3589	−0.0585	0.9997

Table 2.1: Coefficients of the polynomial fit of 3^{rd} degree for the length of the tether per unit height that leads to notable scenarios such as minimum tension, slack, 5%, 10% or 20% increasing tension depending on the relative position.

It is safe to say that these coefficients form a trustworthy approximation function which can be used to compute at each relative position what is the desired length for the tether. This value is the reference to be followed by the proposed system that would actuate to roll or unroll the pulley and therefore extend or stretch the tether.

Having a function is very useful when the system needs to respond quickly, it reduces a lot of the time spent on computations which carry most of the responsibility for the responsiveness of the pulley system.

As expected figure 2.6 shows that the lengths that increase the departure angle and the tension in the UAV are always smaller than the slack lengths. However, these polynomials for bigger relative positions end up becoming useless, this is not shown in the figure even though it happens in the form of an inflexion point, which is expected since it is a third-degree polynomial. The smallest inflexion point is for $l/h \approx 2.05$. A solution can be to use the third-degree polynomial for $l/h \leq 1.95$ and extrapolate for a second-degree polynomial to use when $l/h \geq 2.15$, in between a linear combination of both can be used to smooth the transition.

After the extrapolation is performed it yields the coefficients for the 2^{nd} degree polynomial written in table 2.2.

L	c_1	c_2	c_3	R^2
L_5	0.9594	0.3103	0.1890	0.9998
L_{10}	0.9582	0.2907	0.1990	0.9997
L_{20}	0.9595	0.2630	0.2118	0.9997

Table 2.2: Coefficients of the polynomial fit of 2^{nd} degree extrapolated from the 3^{rd} degree polynomial fit for the length of the tether per unit height that leads to notable scenarios such as 5%, 10% or 20% increasing tension in reference to slack tension depending on the relative position.

By using a simple average as the linear combination to smooth the transition between the first fit and the second one it allows the function to compute values for tether lengths in scenarios where the relation between the horizontal span and the vertical span is even bigger than before. The transition and a reasonable overview of the full final functions are shown in figure 2.7. Finally one must take into account that these functions are approximations, therefore there might be some cases, especially near taut or slack lengths in which the functions may compute a length that is not desirable, this is one of the many reasons why it is for the best to choose working zones in which there is some room for approximation errors since the approach chosen is based on polynomial fits.

2.3.2 Heave Tolerance

There is another issue which is of the utmost importance which is the heave robustness of this system. This means the amount of margin in terms of vertical displacement of the ASV caused by the oscil-

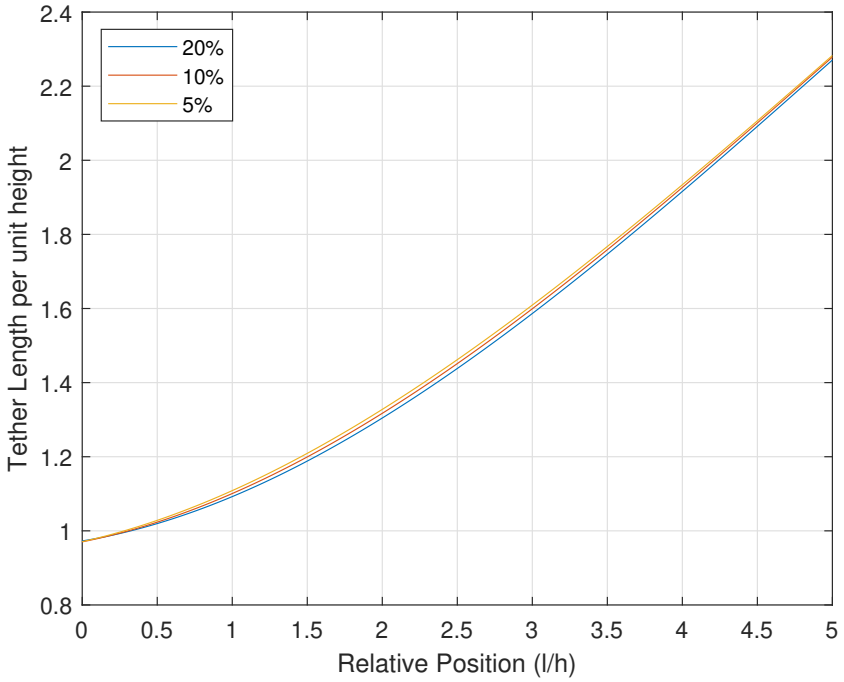

Figure 2.7: Polynomial fit of 2^{nd} and 3^{rd} degree for the length of the tether per unit height that leads to notable scenarios such as 5%, 10% or 20% increasing tension in reference to slack tension depending on the relative position.

lation of the marine surface the system can coop with without either the tether touching the water or becoming taut. One could argue that the system may be able to respond quickly enough to any vertical displacement, however from an engineering point of view any slack or margin that may protect the system, especially in extreme situations, is welcomed. The two extreme outcomes of the surface vehicle being moved up or down, respectively the tether becoming slack or taut, are represented in figure 2.8.

To address this subject a new 2D discretization of the flying space was made but this time computing for each position with a given tether length, defined by the previous functions, how much the ASV can go up or down until it reaches either the slack or the taut condition respectively. There are two notable areas in the flying space in figure 2.9(a) and 2.9(b), the most vertical one and the most horizontal one, in both of them the heave robustness is approximately zero. This happens due to the fact that in those zones the taut length and the slack length are very close to each other, which means that any displacement may lead to fully stretching the cable or turning the departure angle of the cable at the ASV downwards and eventually contact the water. These are not good operating areas, there is not much margin for error, and any mistake will easily lead to stretching too much of the tether and eventually destabilising the aerial vehicle or making it contact with the water. The figure presents a wide range of options for adequate operating points, at least way more than in figure 2.3 for the fixed tether length. A good option might be as far as possible from extreme scenarios either the one related to almost no heave

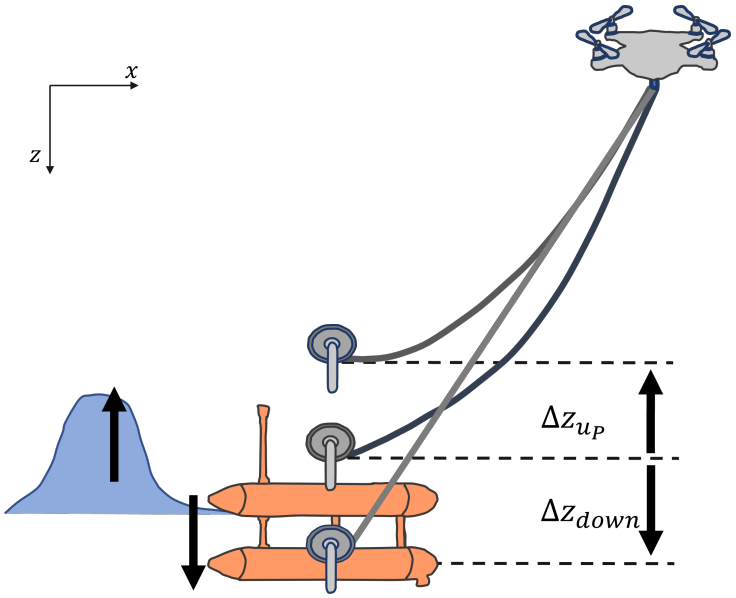

Figure 2.8: Heave impact on the tether. A regular event and the two extreme scenarios due to the heave.

robustness or the ones out of the cable range. Several options present upward robustness of around 2 m and downward robustness of 1.80 m. These values will fluctuate depending on several factors, like the usage of a tether with a different linear mass density or with a bigger maximum length. This means that regardless of the material available or the desired range, new values can and must be calculated, both for the coefficients of the polynomials and for this heave tolerance. To compare the heave robustness for the tether in question for the three functions previously defined, a 2D flying space analysis, presented in figure 2.9, was made for each tension increase, with the upward and downward tolerance for each position represented. The best working zone is one that maximizes both tolerances. As expected the 5% option, because it is closer to slack length, has a better downward motion tolerance, the opposite occurs for the 20% option. The 10% increase from slack tension is the more balanced choice in which generally one can get bigger values for both types of motion. Despite all of this, all three functions present acceptable working zones, it is up to the designer to choose the one that suits better its system. Is power consumption a problem? Then the tension on UAV shall be minimised by choosing a smaller increase from slack tension, the 5% length function. Is upward motion robustness more important than downward, which may mean that it is more of a priority to avoid contact with the water than to avoid fully stretching the tether? The best choice is the 20% tether length function.

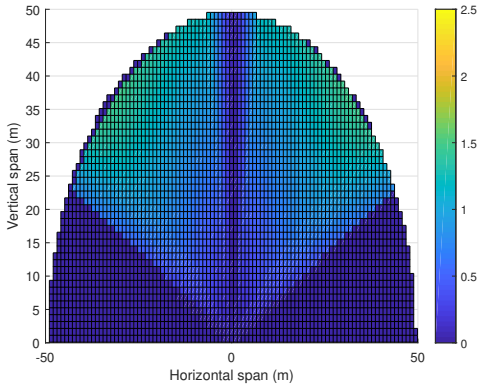

(a) Upward motion, 5% tension increase from slack tension.

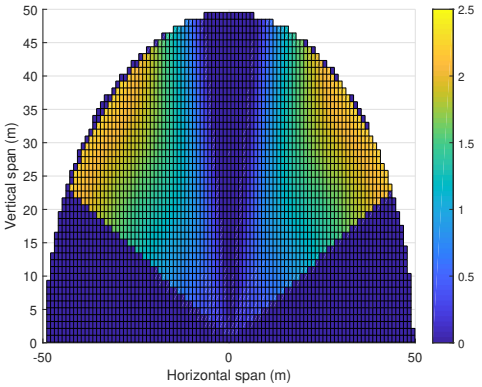

(b) Downward motion, 5% tension increase from slack tension.

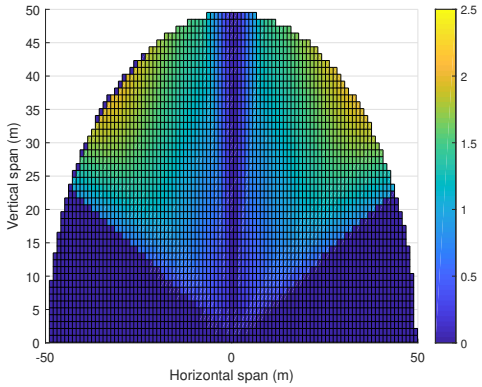

(c) Upward motion, 10% tension increase from slack tension.

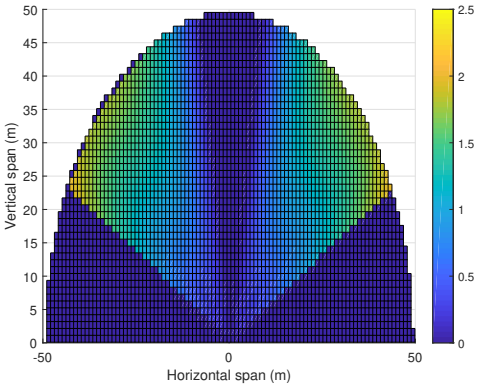

(d) Downward motion, 10% tension increase from slack tension.

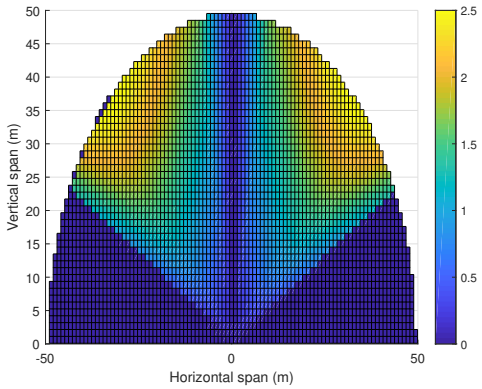

(e) Upward motion, 20% tension increase from slack tension.

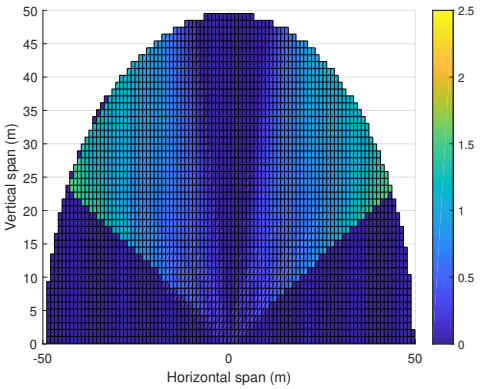

(f) Downward motion, 20% tension increase from slack tension.

Figure 2.9: Upward and downward margins for vertical displacement of the ASV with a tether length fixed and defined for the relative position with no vertical displacement for a 5%, 10% and 20% tension increase compared to the slack length.

3

Unmanned Aerial Vehicle - Modelling and Control

Contents

This chapter describes the model of a quadrotor, which is a type of Unmanned Aerial Vehicle (UAV) with four propellers. Then it is established an inner-loop outer-loop control structure for the vehicle. The theoretical foundation of this chapter is based on the contents present in [30] and [31].

3.1 Quadrotor Model

3.1.1 Notation and Reference Frames

Before describing the quadrotor dynamics, we introduce the reference frames and the notation adopted in this thesis.

There are two important frames: the inertial reference frame $\{\mathrm{I}\}$ which can be fixed anywhere and follows the North-East-Down (NED) convention, and the body-fixed frame $\{\mathrm{B}\}$ which is fixed to the body and follows the same convention. Reference frames are defined by an origin and 3 orthonormal axes. The inertial reference frame $\mathcal{F}_I = \{O_I, \mathbf{x}_I, \mathbf{y}_I, \mathbf{z}_I\}$ and the body-fixed frame $\mathcal{F}_B = \{O_B, \mathbf{x}_B, \mathbf{y}_B, \mathbf{z}_B\}$ are shown in figure 3.1.

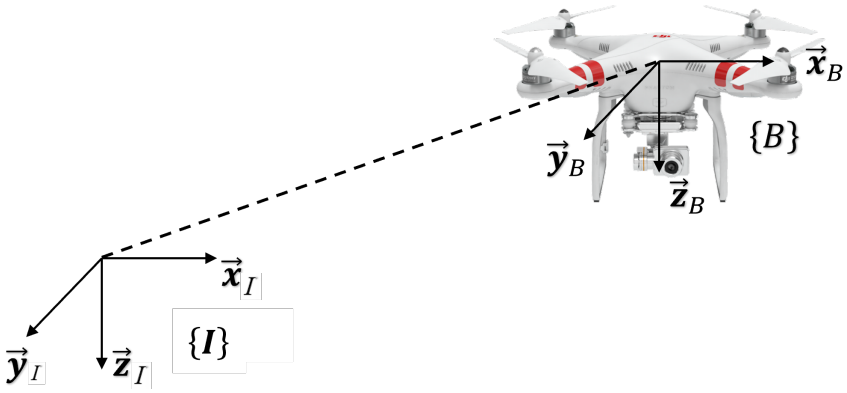

Figure 3.1: Inertial reference frame $\{\mathrm{I}\}$ and body-fixed frame $\{\mathrm{B}\}$.

The position of the origin of the body-fixed frame with respect to the inertial reference frame is given by ${}^{I}p_B \in \mathbb{R}^3$. The orientation of the axis of the body-fixed frame with respect to the inertial reference frame is given by ${}^{I}_{B}R \in \mathbb{SO}^3$, which is yielded by following Z-Y-X convention to apply rotation with Euler angles with $c(\cdot)$ and $s(\cdot)$ being the cosine and sine functions,

$$
{}^{I}_{B}R = R_z(\psi)R_y(\theta)R_x(\phi) = \begin{bmatrix} c(\psi)c(\theta) & c(\psi)s(\theta)s(\phi) - c(\phi)s(\psi) & s(\psi)s(\phi) + c(\psi)c(\phi)s(\theta) \\ c(\theta)s(\psi) & c(\psi)c(\phi) + s(\psi)s(\theta)s(\phi) & c(\phi)s(\psi)s(\theta) - c(\psi)s(\phi) \\ -s(\theta) & c(\theta)s(\phi) & c(\theta)c(\phi) \end{bmatrix}. \tag{3.1}
$$

To simplify the notation consider that $p = {}^{I}p_B$ and $R = {}^{I}_{B}R$.

3.1.2 Quadrotor Kinematics

The kinematics of the quadrotor are given by

$$\dot{p} = Rv \tag{3.2}$$

$$\dot{R} = RS(\omega). \tag{3.3}$$

In this case, it is defined the first derivative of the quadrotor position in the inertial reference frame, where v is the linear velocity and ω the angular velocity, both expressed in the body frame. The $S(\omega)$ is the skew matrix of ω that when multiplied with another vector performs the cross product.

3.1.3 Quadrotor Translational Dynamics

According to Newton's second law, by the conservation of linear momentum, one can write

$$\frac{d}{dt}m\dot{p} = m\ddot{p} = {}^{I}f. \tag{3.4}$$

where m stands for mass and is assumed constant and ${}^{I}f$ denotes the sum of all external forces expressed in the inertial frame.

The same reasoning can be done for the body frame in which case the centripetal term shows up

$$\frac{d}{dt}mRv = {}^{I}f \tag{3.5}$$

$$mR\dot{v} + mRS(\omega)v = {}^{I}f \tag{3.6}$$

$$m\dot{v} + mS(\omega)v = f. \tag{3.7}$$

In this case, the external forces are presented in that frame which is accomplished by $f = R^T\,{}^{I}f$.

If a near hover condition is considered in which aerodynamic drag is neglected as well as other possible disturbances there are only two forces applied to the vehicle, which are its own thrust (T) and the gravitational force, yielding

$$f = -Te_3 + mgR^Te_3 \tag{3.8}$$

$${}^{I}f = mge_3 - TRe_3. \tag{3.9}$$

It is also important to point out that in (3.8) an ideal situation is described, in which the disturbances are not taken into account. In order to do so, the disturbance force component must be added to the

applied forces and (3.9) is rewritten as

$$^{I}f \;=\; mge_3 - TRe_3 + T_V + D, \tag{3.10}$$

where T_V denotes the disturbance created by the tether on the UAV in the inertial frame and D every other disturbance such as the wind. By joining equations (3.4) and (3.10) the equation of motion for translation can be written as

$$m\ddot{p} \;=\; mge_3 - TRe_3 + T_V + D, \tag{3.11}$$

$$\ddot{p} \;=\; ge_3 - \frac{T}{m}Re_3 + \frac{T_V}{m} + \frac{D}{m}. \tag{3.12}$$

3.1.4 Quadrotor Rotational Dynamics

The angular momentum is conserved as well, therefore, because J is constant, any variation is connected to external torques that might be applied to the quadrotor. The angular momentum is given by $RJ\omega$, so its time derivative expressed in the inertial reference frame is given by,

$$\frac{d}{dt}RJ\omega \;=\; RJ\dot{\omega} + RS(\omega)J\omega \;=\; {}^{I}\tau. \tag{3.13}$$

When transformed to the body frame, the expression becomes

$$J\dot{\omega} + S(\omega)J\omega \;=\; \tau. \tag{3.14}$$

The rotational dynamics can be written as

$$J\dot{\omega} \;=\; -S(\omega)J\omega + \tau, \tag{3.15}$$

which resemble the double integrator form of the translational dynamics (3.12) but with the added complexity needed to represent rotational motion.

3.2 Quadrotor Trajectory Tracking Control

The trajectories to be tracked are defined as position vectors $p_d(t) \in \mathbb{R}^3$ that are sufficiently smooth functions of time such that $\dot{p}_d(t)$ and $\ddot{p}_d(t)$ are well defined for all $t > 0$. The chosen control strategy for

trajectory tracking was a hierarchical control strategy. This structure is composed of an outer-loop for the translational dynamics which computes the quadrotor thrust, T, and desired orientation, $R_d e_3$, which in turn feeds the inner-loop which is responsible for controlling the applied torque, τ. In section 3.2.1 and 3.2.2 both loops are studied separately. This section sets the control laws for the vehicle, connecting its translational and orientation dynamics. Figure 3.2 presents the control system structure, which is an inner-loop outer-loop control where the inner part shall be faster than its outer part to get the desired stability for the whole system. This type of hierarchical structure allows designing separately the inner and outer loops as long as the outer-loop feeds the inner-loop with the desired references. For example, at a higher level, it is possible to switch to different Path-following (PF) control laws without changing the inner-loop design. A problem with this approach is that it is harder to analyse its stability.

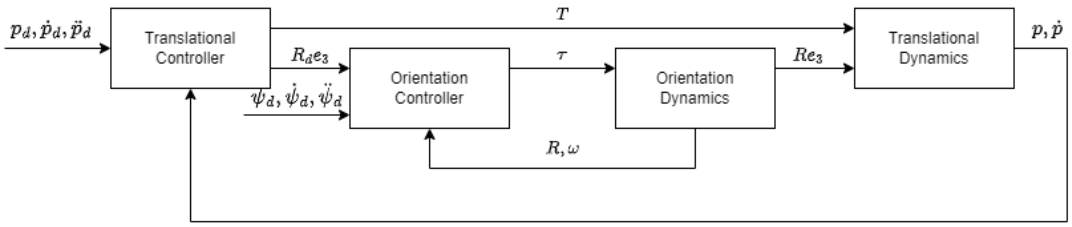

Figure 3.2: Block diagram of the quadrotor trajectory tracking control system.

3.2.1 Translational Controller

In order to define a control law that is able to track a pre-defined trajectory $(p_d(t), \dot{p}_d(t), \ddot{p}_d(t))$, the equation of motion defined in (3.12), neglecting both disturbances terms due to the fact that the controller has no direct knowledge of those, can be simplified to

$$\ddot{p} \;=\; g + u_T + \frac{T_V}{m} + \frac{D}{m}. \tag{3.16}$$

The errors that will feed the controller are

$$\tilde{p}(t) \;=\; p(t) - p_d(t) \tag{3.17}$$

$$\dot{\tilde{p}}(t) \;=\; \dot{p}(t) - \dot{p}_d(t) \tag{3.18}$$

$$\ddot{\tilde{p}}(t) \;=\; \ddot{p}(t) - \ddot{p}_d(t). \tag{3.19}$$

By joining the model from equation (3.12) with the equation (3.19) we can assume

$$\ddot{\tilde{p}}(t) \;=\; g + u_T - \ddot{p}_d(t) + \frac{T_V}{m} + \frac{D}{m}. \tag{3.20}$$

By using a Proportional Integral Derivative (PID) controller the error dynamics (3.19) can be defined as

$$\ddot{\tilde{p}}(t) \;=\; -K_P\tilde{p}(t) - K_I\int_0^t \tilde{p}(\tau)d\tau - K_D\dot{\tilde{p}}(t). \tag{3.21}$$

It can be shown that, with an appropriate choice of gains K_P, K_D and K_I, the system is stable and by means of the integral action $\tilde{p}$ converges to zero even in the presence of constant disturbances T_V and D. Finally, we get the desired control law for u_T in order to follow the translational references,

$$u_T \;=\; -K_P\tilde{p}(t) - K_I\int_0^t \tilde{p}(\tau)d\tau - K_D\dot{\tilde{p}}(t) - g + \ddot{p}_d(t) + \frac{T_V}{m} + \frac{D}{m}. \tag{3.22}$$

The translational dynamics will receive as an input the thrust as a value for the magnitude of the force applied,

$$T = m\|u_T\|. \tag{3.23}$$

The orientation controller will receive the direction in which the thrust should be applied,

$$R_d e_3 = -\frac{u_T}{\|u_T\|}. \tag{3.24}$$

3.2.2 Orientation Controller

The inner-loop receives as an input the desired orientation provided by the translational controller as presented in equation (3.24). This desired orientation is only reflected on the roll ϕ and pitch θ angles since the yaw ψ moves around the body-fixed reference frame z-axis which is always the leading direction of the quadrotor thrust, therefore any kind of variation of this angle will not affect the direction in which the quadrotor moves. It is important to point out that this loop affects the translational dynamics because it will output the new orientation, which is tracking the reference given by the translational controller, that acts as input for the translational dynamics in order to complete the whole system's loop. The previous statements sets this controller's references as $\lambda_d = (\phi_d, \theta_d, \psi_d)$, in which ψ_d is pre-defined and the pair ϕ_d and θ_d is computed from the desired orientation $R_d e_3$,

$$R_d e_3 = R_z(\psi)R_y(\theta)R_x(\phi)e_3 = R_z(\psi)\begin{bmatrix} cos\phi sin\theta \\ -sin\phi \\ cos\phi cos\theta \end{bmatrix}. \tag{3.25}$$

Now if it is assumed for example a fixed value for the yaw angle, $\psi = 0$ rad, it is easy to compute the

desired angles for roll and pitch,

$$\psi = 0\ rad \tag{3.26}$$

$$\theta_d = arctan\left(\frac{R_{d13}}{R_{d33}}\right) rad \tag{3.27}$$

$$\phi_d = arctan\left(\frac{-R_{d23}}{\sqrt{R_{d13}^2 + R_{d33}^2}}\right) rad. \tag{3.28}$$

The error dynamics considered to define the attitude controller are

$$\tilde{\lambda}(t) \ = \ \lambda(t) - \lambda_d(t) \tag{3.29}$$

$$\dot{\tilde{\lambda}}(t) \ = \ \dot{\lambda}(t) - \dot{\lambda}_d(t) \tag{3.30}$$

$$\ddot{\tilde{\lambda}}(t) \ = \ \ddot{\lambda}(t) - \ddot{\lambda}_d(t) = \ \tau - \ddot{\lambda}_d(t). \tag{3.31}$$

where the attitude dynamics were linearized about the hover condition. The control law ends up being very similar to the one from the translational controller,

$$\tau \ = \ -K_P\tilde{\lambda}(t) - K_D\dot{\tilde{\lambda}}(t) + \ddot{\lambda}_d(t). \tag{3.32}$$

4

Autonomous Surface Vehicle - Modelling and Control

Contents

This chapter starts by presenting the reference frames and notation used to describe the Autonomous Surface Vehicle (ASV) dynamic model. Then a general model of a marine vehicle, which can also be an Autonomous Underwater Vehicle (AUV), is introduced. This is followed by a simplification concerning the Degrees of freedom (DOF) that are relevant for the ASV scenario, constrained to the two-dimensional (2D) plane. Finally, two control laws for the surge speed and the yaw rate of the surface vehicle are presented.

4.1 Autonomous Surface Vehicle Model

4.1.1 Notation and Referential Frames

Similarly to what was done in Chapter 3 the coordinate frames that are going to be used must be defined. There are two reference frames, the Inertial reference frame {I} with basis $\mathcal{F}_I = \{O_I, \mathbf{x}_I, \mathbf{y}_I, \mathbf{z}_I\}$, aligned with the North-East-Down (NED) convention, and the Body-fixed frame {B} with basis $\mathcal{F}_B = \{O_B, \mathbf{x}_B, \mathbf{y}_B, \mathbf{z}_B\}$ which is fixed to the body center of mass, the x_B is the longitudinal axis which is directed from aft to fore, the y_B is the transversal axis which is directed to starboard and z_B is the normal axis which is directed downwards. A representation of both reference frames is presented in figure 4.1.

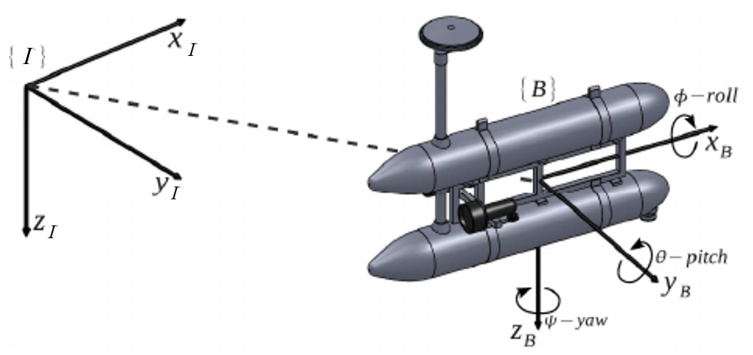

Figure 4.1: Inertial reference frame {I} and body-fixed frame {B} (adopted from [4]).

To model a marine vehicle it is necessary to account for its 6 DOF, three coordinates for position (x, y, z), surge, sway and heave, and another three for orientation (ϕ, θ, ψ), roll, pitch and yaw. In table 4.1 it is represented the Society of Naval Architects & Marine Engineers (SNAME) notation used for marine vehicles, as it is used in [32].

	Forces and torques	Linear and angular velocities	Position and orientation
Motions in the x direction (surge)	X	u	x
Motions in the y direction (sway)	Y	v	y
Motions in the z direction (heave)	Z	w	z
Rotation about the x axis (roll, heel)	K	p	ϕ
Rotation about the y axis (pitch, trim)	M	q	θ
Rotation about the z axis (yaw)	N	r	ψ

Table 4.1: SNAME notation for marine vehicles.

This notation can also be represented in a vectorial form, which can ease the process of modelling the marine vehicle. Those vectors are,

- $\eta_1 = [x, y, z]^T$, which is the position of $\{\mathsf{B}\}$ expressed in $\{\mathsf{I}\}$.
- $\eta_2 = [\phi, \theta, \psi]^T$, which is the orientation of $\{\mathsf{B}\}$ with respect to $\{\mathsf{I}\}$.
- $\nu_1 = [u, v, w]^T$, which is the linear velocity of $\{\mathsf{B}\}$ relative to $\{\mathsf{I}\}$, expressed in $\{\mathsf{B}\}$.
- $\nu_2 = [p, q, r]^T$, which is the angular velocity of $\{\mathsf{B}\}$ relative to $\{\mathsf{I}\}$, expressed in $\{\mathsf{B}\}$.
- $\tau_1 = [X, Y, Z]^T$, which is the forces acting on the body in $\{\mathsf{B}\}$.
- $\tau_2 = [K, M, N]^T$, which is the torques acting on the body in $\{\mathsf{B}\}$.

4.1.2 Kinematics of a Marine Vehicle

As it is presented in [32], the kinematics of a generic marine vehicle are given by,

$$\dot{\eta} = J(\eta)\nu, \tag{4.1}$$

this can be expanded as,

$$\begin{bmatrix} \dot{\eta}_1 \\ \dot{\eta}_2 \end{bmatrix} = \begin{bmatrix} {}^I_B R(\eta_2) & 0_{3\times3} \\ 0_{3\times3} & Q(\eta_2) \end{bmatrix} \nu. \tag{4.2}$$

The orientation of the axis of the body-fixed frame of the ASV with respect to the inertial reference frame is given by ${}^I_B R \in \mathbb{SO}^3$, which was expanded in Chapter 3 in (3.1).

The matrix $Q(\eta_2)$ is a transformation matrix that relates the angular velocities, $\nu_2 = [p, q, r]^T$ and the vehicle orientation with respect to the inertial frame, which is given by,

$$Q(\eta_2) = \begin{bmatrix} 1 & s(\phi)t(\theta) & c(\phi)t(\theta) \\ 0 & c(\phi) & -s(\phi) \\ 0 & s(\phi)/c(\theta) & c(\phi)/c(\theta) \end{bmatrix}, \tag{4.3}$$

with $t(\cdot)$ being the tangent function. It is noticeable that there is a singularity in equation (4.3) for the pitch angle, where $\theta \neq \pm\pi\, rad$. This would not be a problem if a quaternion representation is used,

nonetheless, this comes only as a mere mathematical issue since the working zone for the vehicle in study will be for pitch and roll to be near zero radians, $\theta \approx 0\,rad$ and $\phi \approx 0\,rad$.

4.1.3 Dynamics of a Marine Vehicle

In [33], the dynamics of a generic marine vehicle are given by,

$$M_{RB}\dot{\nu} + C_{RB}(\nu)\nu = \tau_{RB}, \tag{4.4}$$

where M_{RB} is the rigid-body mass matrix, C_{RB} is the rigid-body Coriolis and centripetal matrix due to the rotation of the body-fixed frame with respect to the inertial frame and the τ_{RB} is the joint vector of the forces and torques acting on the body in its fixed frame, $\tau_{RB} = [X, Y, Z, K, M, N]^T$. The term τ_{RB} can also be described as the sum of external interactions with the vehicle,

$$\tau_{RB} = \tau + \tau_A + \tau_D + \tau_R + \tau_{dist}, \tag{4.5}$$

where the τ is the forces and torques that are input to the system by thrusters for example, $\tau_A = -M_A\dot{\nu} - C_A(\nu)\nu$ is the term related to hydrodynamic added mass, the $\tau_D = -D(\nu)\nu$ is the hydrodynamic drag, lift and friction effects on the vehicle, where $D(\nu)$ is strictly positive, the term that includes the impact of the gravity and fluid density $\tau_R = -g(\eta)$ and finally, τ_{dist} is the disturbances term that might include for example the wind and the waves. Therefore, the compact notation to describe the dynamics of the marine vehicle are,

$$M\dot{\nu} + C(\nu)\nu + D(\nu)\nu + g(\nu) = \tau + \tau_{dist}, \tag{4.6}$$

where $M = M_{RB} + M_A$ which is constant and positive definite, $z^T M z > 0, \forall_{z \in \mathbb{R}^6}$ and $\dot{M} = 0_{6\times 6}$, and $C(\nu) = C_{RB}(\nu) + C_A(\nu)$ which is skew-symmetrical, $C(\nu) = -C^T(\nu), \forall_{\nu \in \mathbb{R}^6}$.

4.1.4 Simplified Equations of Motion

The previous equations for the kinematics and dynamics of marine vehicles were general for any kind of vehicle. In this section, it is defined a set of equivalent equations, as in [34], specific for the surface case of those vehicles, with all the necessary simplifications. The working zone is approximately a 2D plane, which means that there is only 3 DOF which are $[x, y, \psi]^T$, it is considered that $\theta \approx 0\,rad$, $\phi \approx 0\,rad$ and $z \approx 0$. The kinematics of the ASV are,

$$\begin{bmatrix} \dot{x} \\ \dot{y} \end{bmatrix} = \begin{bmatrix} cos(\psi) & -sin(\psi) \\ sin(\psi) & cos(\psi) \end{bmatrix} \begin{bmatrix} u \\ v \end{bmatrix}, \tag{4.7}$$

$$\dot{\psi} = r. \tag{4.8}$$

In this equations, u and v are the surge speed and the sway speed, respectively, both in the body-fixed frame, x and y define the 2D position in the inertial frame with ψ defining orientation in the same frame and r the angular speed. If there is a constant and irrotational ocean current $[u_c, v_c]^T \neq 0$, both surge and sway speed are $u = u_r + u_c$ and $v = v_r + v_c$, with u_r and v_r being the relative body-current linear velocities.

In what concerns the dynamics, by using the same simplifications, the new equations are,

$$m_u \dot{u}_r - m_v v_r r + d_{u_r} u_r = \tau_u, \tag{4.9}$$

$$m_v \dot{v}_r + m_u u_r r + d_{v_r} v_r = 0, \tag{4.10}$$

$$m_r \dot{r} - m_{uv} u_r v_r + d_r r = \tau_r, \tag{4.11}$$

where the τ_u is the external force in surge motion and τ_r is the external torque along the z axis, and also,

$$\begin{aligned} m_u &= m - X_{\dot{u}}, \quad d_{u_r} = -X_u - X_{|u|u}|u_r|, \\ m_v &= m - Y_{\dot{v}}, \quad d_{v_r} = -Y_v - Y_{|v|v}|v_r|, \\ m_r &= I_z - N_{\dot{r}}, \quad d_r = -N_r - N_{|r|r}|r|, \\ m_{uv} &= m_u - m_v, \end{aligned} \tag{4.12}$$

with m_u, m_v, m_r and m_{uv} representing the mass and hydrodynamic added mass and d_u, d_v and d_r being the hydrodynamic damping effects. These set equations assume that the ASV is neutrally buoyant and that its centre of buoyancy coincides with the centre of gravity.

4.2 Autonomous Surface Vehicle Control

The proposed control scheme is to control both linear and angular velocities, respectively the surge speed u and the yaw rate r. In this section a control law is derived for each one of the system's inputs, the force along the surge axis τ_u and the torque along the body z-axis, to make $[u, r]^T$ converge to the desired $[u_d, r_d]^T$. The proposed control structure is displayed in figure 4.2.

4.2.1 Surge Speed Control

In order to control the surge speed of the ASV one has to use its dynamics described in equation (4.9). It is considered that the sway speed is approximately zero, $v \approx 0$. Therefore, the dynamics can be rewritten as,

$$\dot{u}_r = \frac{1}{m_u}(\tau_u - d_{u_r} u_r). \tag{4.13}$$

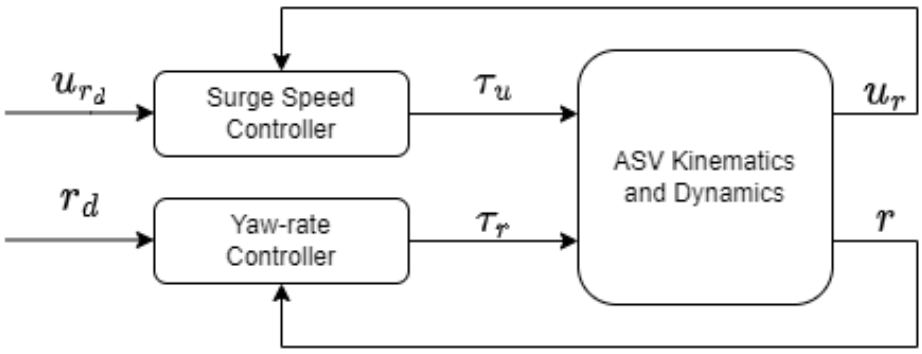

Figure 4.2: Block diagram of the ASV control system.

The errors to consider are,

$$\tilde{u}_r(t) = u_r(t) - u_{r_d}(t) \tag{4.14}$$

$$\dot{\tilde{u}}_r(t) = \dot{u}_r(t) - \dot{u}_{r_d}(t) \tag{4.15}$$

If one joins the equation (4.13) with the equation (4.21) it yields,

$$\dot{\tilde{u}}_r(t) = \frac{1}{m_u}(\tau_u - d_{u_r} u_r) - \dot{u}_{r_d}(t), \tag{4.16}$$

by using a Proportional Integral (PI) controller the error defined in equation (4.21) is

$$\dot{\tilde{u}}_r(t) = -K_P \tilde{u}_r(t) - K_I \int_0^t \tilde{u}_r(\tau)\, d\tau, \quad K_P, K_I > 0, \tag{4.17}$$

and, finally, by inserting it in (4.22) and by rearranging it, we get the desired control law,

$$\tau_u = m_u \left[- K_P \tilde{u}_r(t) - K_I \int_0^t \tilde{u}_r(\tau) d\tau + \dot{u}_{r_d}(t) \right] + d_{u_r} u_r. \tag{4.18}$$

4.2.2 Yaw Rate Control

Following the same strategy to control the yaw rate, by considering the ASV dynamics in equation (4.11) and also the sway speed to be approximately zero, $v \approx 0$. Then rewriting it as,

$$\dot{r} = \frac{1}{m_r}(\tau_r - d_r r). \tag{4.19}$$

The errors to consider are,

$$\tilde{r}(t) = r(t) - r_d(t) \tag{4.20}$$

$$\dot{\tilde{r}}(t) = \dot{r}(t) - \dot{r}_d(t) \tag{4.21}$$

If one joins the equation (4.13) with the equation (4.21) it yields,

$$\dot{\tilde{r}}(t) = \frac{1}{m_u}(\tau_r - d_r r) - \dot{r}_d(t), \tag{4.22}$$

by using a PI controller the error defined in equation (4.21) is

$$\dot{\tilde{r}}(t) = -K_P \tilde{r}(t) - K_I \int_0^t \tilde{r}(\tau) d\tau, \quad K_P, K_I > 0, \tag{4.23}$$

and, finally, by inserting it in (4.22) and by rearranging it, we get the desired control law,

$$\tau_r = m_u \Big[- K_P \tilde{r}(t) - K_I \int_0^t \tilde{r}(\tau)\, d\tau + \dot{r}_d(t) \Big] + d_r r \tag{4.24}$$

It is important to point out that there is a feedforward term in both control laws, $\dot{u}_{r_d}(t)$ and $\dot{r}_d(t)$, which would vanish in a situation that the desired surge speed and yaw rate are to be constant, which is a usual scenario for this kind of applications and missions.

5

Cooperative Path-following

Contents

In this chapter, a Path-following (PF) strategy is assigned for both vehicles, the ASV and the UAV. Then a cooperation algorithm is introduced to perform PF as a team while being connected by a tether.

5.1 Path-following

The assignment of a mission for the vehicles to perform is the assignment of a path to be followed. As previously stated there are several possible strategies to accomplish such a goal. This chapter follows a strategy that converts Trajectory Tracking (TT) into PF with the help of a virtual target. This creates a less demanding scenario for any vehicle, it is only TT when the vehicle is close to the virtual target, otherwise, the references are updated to improve the vehicle's ability to follow the path. The definition of this virtual target is based on [15] which is about creating two control laws, one to define the virtual target evolution along the pre-defined path and another to define a reference to follow by the vehicle based on the position and motion of the target. The approach to create this target is similar for both vehicles, however, the references for each controller are different. This is an advantage of this method, it can be used for a wide range of vehicles whichever references are to be followed.

The idea is to consider a vehicle with known kinematics and dynamics, and also a virtual target which position is defined by $p_d(\gamma)$, which is $p_d(\gamma) \in \mathbb{R}^2$ for the ASV and $p_d(\gamma) \in \mathbb{R}^3$ for the UAV, with a desired speed of $v_d(\gamma) \in \mathbb{R}$. This position and desired speed are parameterized by $\gamma \in \mathbb{R}$, which represents each instant in time through the trajectory. The goal is to create control laws for $\mathbf{u}_d$ and $\dot{\gamma}$, which are the reference speed $[u_d, r_d]^T$ for the ASV and $[p_d, \dot{p}_d, \ddot{p}_d]^T$ for the UAV, and the rate of evolution of the virtual target along the path. Ultimately this laws shall lead to $||p(t) - p_d(\gamma(t))|| \to 0$ and to $\dot{\gamma}(t) \to 1$ as time goes by, $t \to \infty$.

5.1.1 Autonomous Surface Vehicle Path-following Control Design

The position error in the body-fixed frame of the ASV is given by,

$$\tilde{p} = {}^B_I R(\psi)(p(t) - p_d), \tag{5.1}$$

therefore its first derivative is

$$\dot{\tilde{p}} = {}^B_I \dot{R}(\psi)(p(t) - p_d) + {}^B_I R(\psi)(\dot{p}(t) - \dot{p}_d). \tag{5.2}$$

This derivative can be simplified by defining the rotation matrix derivative as

$${}^B_I \dot{R} = -S(r) {}^B_I R, \tag{5.3}$$

where the $S(r)$ is the skew-symmetric matrix for the yaw rate, which means that

$$S(r) = \begin{bmatrix} 0 & -r \\ r & 0 \end{bmatrix}. \tag{5.4}$$

It is also known that the linear velocity in the body-fixed frame is given by

$$v = {}^{B}_{I}R\dot{p}(t) = v_r + {}^{B}_{I}Rv_c, \tag{5.5}$$

it is important to remember that v_r is related to the body-fixed frame, v_c is the ocean currents speed expressed in the inertial frame. By replacing (5.3) and (5.5) into (5.2) it yields

$$\dot{\tilde{p}} = -S(r)\tilde{p} + v_r + {}^{B}_{I}Rv_c - {}^{B}_{I}R(\psi)\dot{p}_d. \tag{5.6}$$

Now that the errors are defined it is important to manipulate the expressions in order to define the control laws for the surge speed and yaw rate references. To do so a constant vector is introduced $\boldsymbol{\delta} = [0, \delta]^T, \delta < 0$,

$$\dot{\tilde{p}} = -S(r)(\tilde{p} - \boldsymbol{\delta}) - S(r)\boldsymbol{\delta} + \begin{bmatrix} u \\ v \end{bmatrix} + {}^{B}_{I}Rv_c - {}^{B}_{I}R(\psi)\dot{p}_d \tag{5.7}$$

$$= -S(r)(\tilde{p} - \boldsymbol{\delta}) + \begin{bmatrix} 0 \\ \delta r \end{bmatrix} + \begin{bmatrix} u \\ v \end{bmatrix} + {}^{B}_{I}Rv_c - {}^{B}_{I}R(\psi)\dot{p}_d \tag{5.8}$$

$$= -S(r)(\tilde{p} - \boldsymbol{\delta}) + \Delta u + \begin{bmatrix} 0 \\ v \end{bmatrix} + {}^{B}_{I}Rv_c - {}^{B}_{I}R(\psi)\dot{p}_d. \tag{5.9}$$

where $u = [u_r, r]^T$ and $\Delta = \left[\begin{smallmatrix} 1 & 0 \\ 0 & -\delta \end{smallmatrix}\right]$. Notice that by introducing δ, the virtual input u appears multiplied by the non-singular matrix Δ, meaning that it can be used directly to guarantee convergence of $\tilde{p}$ to $\boldsymbol{\delta}$. The last term of (5.9) has the first derivative of the virtual target's position which can be acquired via chain rule,

$$\dot{p}_d = \frac{\partial p_d(\gamma)}{\partial \gamma}\dot{\gamma}, \tag{5.10}$$

this allows us to write (5.9) as,

$$\dot{\tilde{p}} = -S(r)(\tilde{p} - \boldsymbol{\delta}) + \Delta u + \begin{bmatrix} 0 \\ v \end{bmatrix} + {}^{B}_{I}Rv_c - {}^{B}_{I}R(\psi)\frac{\partial p_d(\gamma)}{\partial \gamma}\dot{\gamma}. \tag{5.11}$$

As said earlier, to perform the PF one needs to define the references to track but also the evolution of the virtual target through time. The references are given by

$$u_d = \Delta^{-1}\bigg(- K_k(\tilde{p} - \boldsymbol{\delta}) - \begin{bmatrix} 0 \\ v \end{bmatrix} + {}^{B}_{I}Rv_c - {}^{B}_{I}R(\psi)\frac{\partial p_d(\gamma)}{\partial \gamma}\dot{\gamma}\bigg), \tag{5.12}$$

where $K_k \succeq 0$ and $K_k = \begin{bmatrix} k_x & 0 \\ 0 & k_y \end{bmatrix}$.

The approach for the virtual target is to have an entity that dynamically defines the values for u_d by moving along the pre-defined path at a pre-specified speed profile when the position error between the vehicle and its target is small, the meaning of being small has to be defined by the designer which has to be adapted for each different object and environment. However, when the error is big the target must move slowly and at some point even stop to wait for the vehicle to get closer to it and therefore converge to the path. The first derivative of the virtual target, $\dot{\gamma}$, is specified as a function of the distance between the vehicle and the target,

$$\dot{\gamma}_{REF} = \begin{cases} 0 & ||p(t) - p_d(\gamma)|| \geq d \\ e^{\frac{||p(t)-p_d(\gamma)||^2}{||p(t)-p_d(\gamma)||^2 - d^2}} & ||p(t) - p_d(\gamma)|| < d \end{cases}, \tag{5.13}$$

where d is the value for the distance from which the virtual target stops and simply waits for the vehicle to get closer. However, to implement this strategy for the evolution of the virtual target depending only on the distance between the actual vehicle and the target, one has to account for noisy position measurements either from odometry or the Global Positioning System (GPS). To do so a first-order system can be used, which ends up filtering the high-frequency noise present in the input, to define $\ddot{\gamma}$,

$$\ddot{\gamma} = -K_V(\dot{\gamma} - \dot{\gamma}_{REF}). \tag{5.14}$$

5.1.2 Unmanned Aerial Vehicle Path-following Control Design

As referred to in Chapter 1 the type of algorithm that suits each vehicle is different, for the ASV the TT is not a good choice, it is too demanding for the responsiveness of the vehicle regarding the environment where it is operating, the natural choice is PF which is a much more tolerant type of algorithm that constantly adapts to the current situation of the vehicle. Despite this limitation for the marine vehicle the same cannot be argued for the aerial one, the UAV deals with the TT algorithms acceptably well. The fact that one wants to make both vehicles cooperate is what makes it almost mandatory to use PF for the whole system, a fixed target for each instant will not be effective, there can be a fixed trajectory, p_d which has to be in C^2, but there must also be a virtual target that dynamically updates its position for the vehicles to receive through time the references to be followed. A controller that can track a pre-defined trajectory for a set of given desired positions, velocities and accelerations is defined in Chapter 3. By joining this control strategy with a virtual target approach, similar to the one designed for the ASV that selects which reference the vehicle must track, it is possible to perform the PF and also do so in a cooperative scenario. The evolution of the virtual target is defined by a structure equal to (5.13). The errors which are going to be tracked by the UAV control structure are in (3.17), (3.18) and (3.19). However the desired references can be rewritten as a function of the virtual target parameter γ,

$$p_d = p_d(\gamma) \tag{5.15}$$

$$\dot{p}_d = \frac{\partial p_d(\gamma)}{\partial \gamma}\dot{\gamma} \tag{5.16}$$

$$\ddot{p}_d = \frac{\partial}{\partial t}\left(\frac{\partial p_d(\gamma)}{\partial \gamma}\dot{\gamma}\right) = \frac{\partial^2 p_d(\gamma)}{\partial \gamma^2}\dot{\gamma}^2 + \frac{\partial p_d(\gamma)}{\partial \gamma}\ddot{\gamma}. \tag{5.17}$$

The terms $\ddot{\gamma}$ and $\dot{\gamma}_{REF}$ are defined as in (5.14) and in (5.13) respectively.

5.2 Cooperation between ASV and UAV

At this point, each vehicle has the capability of individually following a path given a virtual target which depends on their distance to the intended route. For any mission to be cooperative a synchronization protocol among vehicles shall be set. The existence of a virtual target streamlines this process because it can be manipulated depending on how much out of sync the vehicles are. At each instant of time, each vehicle has a value for γ that represents where in the initial desired trajectory they are at that moment, the synchronization is measured as the difference between those γ. This raises some problems, the value for γ is intrinsic for each vehicle which means that communication is needed either for a centralized approach, to communicate with a central computer where decisions are made, or for a decentralized one, to communicate between vehicles and to locally make decisions. As it was disscussed in Chapter 1 communication can be a problem, especially in situations where it is expensive, for example, it drains a lot of energy which is scarce for a UAV, or with mechanisms that are not fast and frequent enough which can bring some inaccuracy on the messages which are being transmitted, for example between underwater vehicles when it is used acoustic methods. For these reasons, communication is usually approached as being discrete and there is a need to be able to select the best moments to send a message. Luckily we are using a tether which allows constant communication, as continuous as it can be, for a much lower cost. Therefore, in this Chapter is defined a control structure that is able to adapt the values of $\dot{\gamma}$ to achieve synchronization and ultimately, a cooperative mission. The chosen strategy to ensure Cooperative Path-following (CPF) is inspired in [17]. Although in the present case, the method is applied to two vehicles only, we present the results in their general form for a multi-agent graph topology. The communication network between vehicles can be described as a graph $\mathcal{G}(\mathcal{V}, \mathcal{E}, \mathcal{A})$, where $\mathcal{V}$ is a set of nodes, in this case, a set of $n \in \mathbb{N} \setminus \{1\}$ vehicles, also $\mathcal{E}$ defines the edges that connects each node to another, which means that for any ϵ_{ij} it is told that the vehicle i is connected to the vehicle j which is not necessarily guaranteed for the other way around, and the $\mathcal{A}$ is an adjacency matrix that can be weighted. It is also useful to define for each vehicle a vector with the information of which vehicles can send information into the vehicle i, $\mathcal{N}_i^{in}$ and to which vehicles the vehicle i is able to send information,

$\mathcal{N}_i^{out}$. Regarding the scenario in study the graph is undirected which means that $\mathcal{N}_i^{in} = \mathcal{N}_i^{out}$. It is also useful to talk about the degree matrix, D, which is a diagonal matrix that tells how many edges are connected to each node. The Laplacian matrix is defined as $L = D - \mathbb{A}$. The goal is to create a control law for correction of $\dot{\gamma}$, defined as $v^c = [v_1^c, \ldots, v_N^c]^T$ for each vehicle i, with $i \in \mathbb{N}$. This law has to bring $|\gamma_i - \gamma_j| \to 0$, $\forall j \in \mathcal{N}_i^{in}$, and therefore, $\dot{\gamma}^c \to 0$ when all γ values, the considered state for the vehicles, are equal. The first step is to define the error vector as $\xi = [\xi_1, ..., \xi_N]^T$, which is given by

$$\xi_i = \sum_{j \in \mathcal{N}_i^{in}} a_{ij}(\gamma_i - \gamma_j), \tag{5.18}$$

this can be represented more compactly as,

$$\xi = L\boldsymbol{\gamma}, \tag{5.19}$$

where L is the Laplacian matrix and $\boldsymbol{\gamma}$ is a vector that represents the state of each vehicle i regarding the value of γ, $\boldsymbol{\gamma} = [\gamma_1, \ldots, \gamma_N]^T$. The proposed control law for v_i^c can be written as,

$$v_i^c = -k_i \sum_{j \in \mathcal{N}_i^{in}} a_{ij}(\gamma_i - \gamma_j), \tag{5.20}$$

and in compact form as,

$$v^c = -K\xi = -KL\boldsymbol{\gamma}, \tag{5.21}$$

where $0 < K \leq 1$ is a proportional gain. This control law yields

$$\dot{\boldsymbol{\gamma}}^{\boldsymbol{c}} = \dot{\boldsymbol{\gamma}} + v^c, \tag{5.22}$$

where $\dot{\boldsymbol{\gamma}}^{\boldsymbol{c}} = [\dot{\gamma}_1^c, \ldots, \dot{\gamma}_N^c]^T$ are the corrected virtual targets speed. A diagram representing the control structure that is going to be implemented in the following Chapters to accomplish the cooperative mission between the marine and the aerial vehicle connected by a tether is included in figure 5.1.

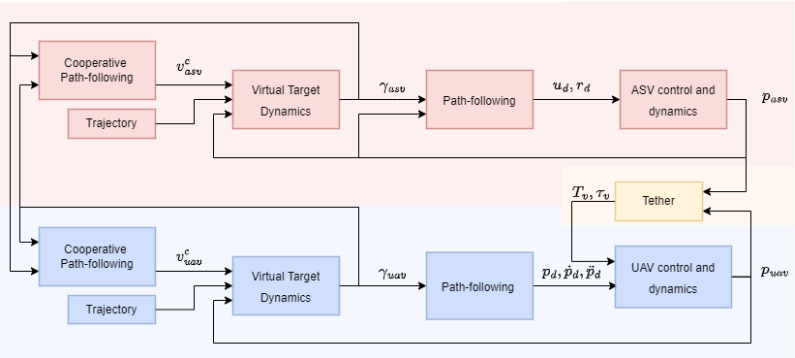

Figure 5.1: Final CPF architecture.

6

Cooperative System Simulation

Contents

In this chapter, the results are presented. Firstly, individual missions are simulated in *MATLAB*, in ideal scenarios, for each vehicle and then the generated data will be analyzed. Then a cooperative mission is launched with the same purpose but with a non-ideal variable, a noisy measurement of the position of the vehicles. The second part of this chapter seeks to simulate the same mission in *Gazebo* with resources from Dynamical Systems and Ocean Robotics Laboratory (DSOR) and a new plug-in created to simulate the tether.

6.1 Single Unmanned Aerial Vehicle Mission

The mission is to start an $1.282\,kg$ UAV hovering at position $[x, y, z] = [1, 1, 2]\,m$ and then to make it follow its virtual target along the predefined path, which is a lawn mower, with a speed profile of $0.5\,m\,s^{-1}$. There is a constant wind disturbance of $[-2, 0, 0]\,N$. The selected gains for the outer-loop of the UAV controller from (3.22) are $K_P = 1.5$, $K_I = 0.2$ and $K_D = 1.5$. For the inner-loop of the UAV controller from (3.32) are $K_P = 10$ and $K_D = 10$. The inner loop gains are much greater than the outer loop's which is justified by the fact that to get this inner-loop and outer-loop structure working properly the inner loop must be faster than the outer loop. Figure 6.1 represents how the UAV follows the path as well as the virtual target, the green point, for each instant of time.

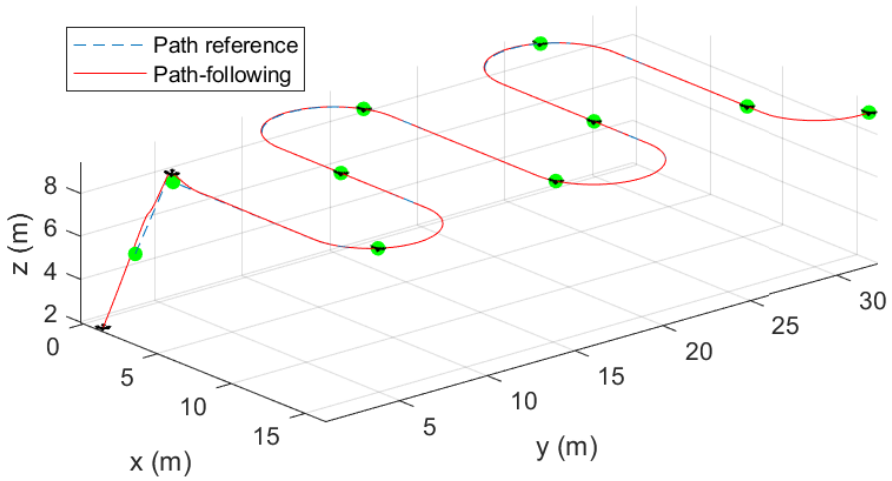

Figure 6.1: Single UAV Lawn-mowing Mission.

Another confirmation that the UAV can follow the intended path with the desired speed profile is in figure 6.2, the distance between the vehicle and its virtual target is kept below 10 cm and the linear velocities are the ones pre-specified both in the straight and curve lines.

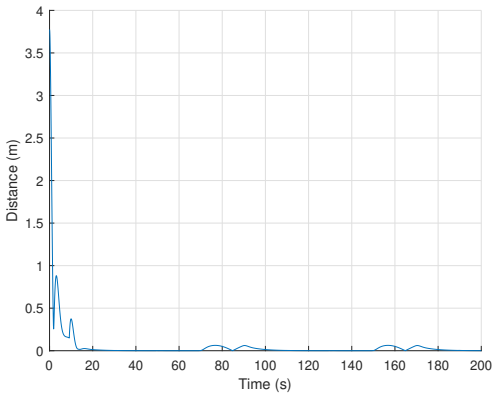

(a) Distance to the virtual target.

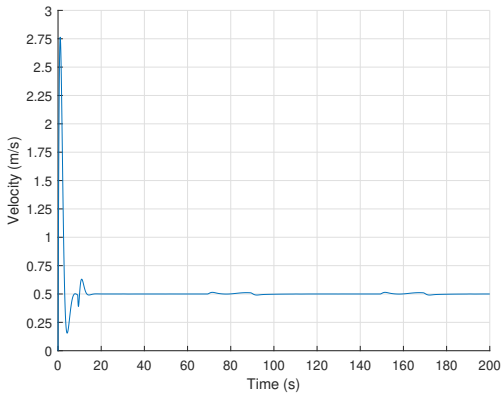

(b) UAV linear velocity.

Figure 6.2: Single UAV Lawn-mowing Mission - distance to the virtual target and linear velocity along the mission.

The inner loop also behaves as expected by tracking accurately the desired attitude for the aircraft, both ϕ and θ. This is shown in figure 6.3.

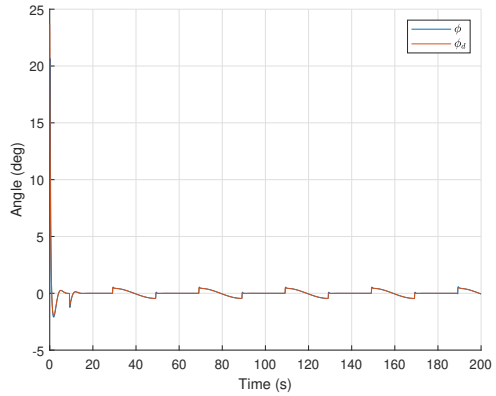

(a) ϕ reference tracking.

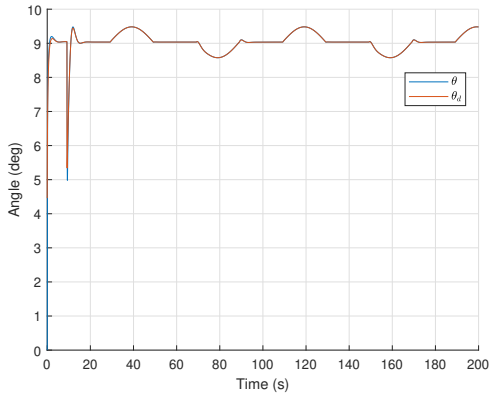

(b) θ reference tracking.

Figure 6.3: Single UAV Lawn-mowing Mission - desired attitude tracking by the inner-loop of the UAV controller.

Regarding the Path-following (PF) algorithm it can be seen in figure 6.4 that $\dot{\gamma}$ converges to 1, which means that γ is progressing at the same speed as the intended trajectory would through time. It is also important to point out that for distances between the vehicle and its virtual target greater than or equal to $5\,m$ the virtual target stops and waits for the real vehicle. The gain for the expression presented in

(5.14) is $K_V = 1$.

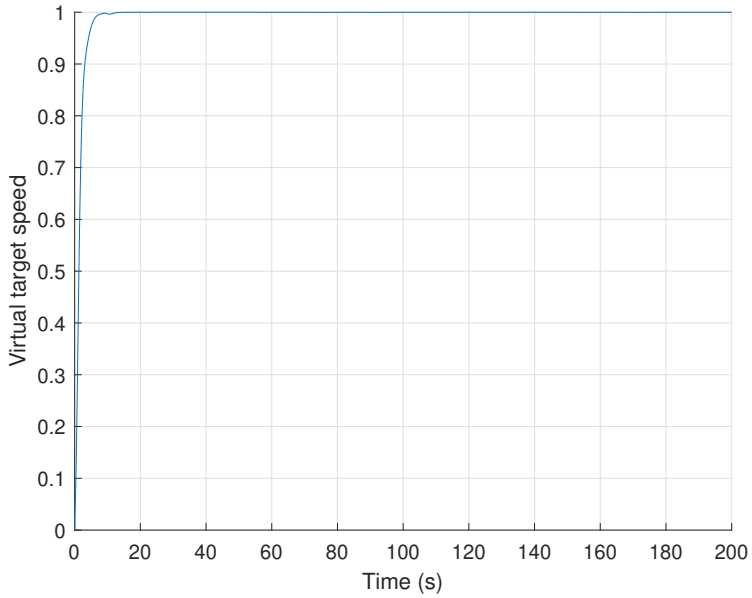

Figure 6.4: Single UAV Lawn-mowing Mission - virtual target speed $\dot{\gamma}$.

In what concerns the applied thrust by the UAV the evolution of the absolute value of each force applied to the vehicle is presented in figure 6.5, which are in this case: the gravitational force, a wind constant disturbance and the force to accelerate the vehicle, but also the thrust that the vehicle must generate to compensate the first and the second and still be able to move as intended.

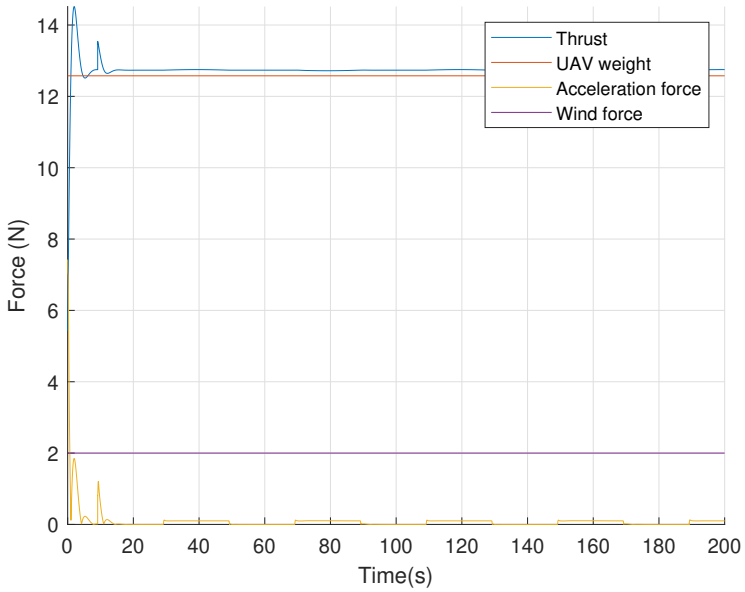

Figure 6.5: Single UAV Lawn-mowing Mission - absolute value of the forces applied to the vehicle.

6.2 Single Autonomous Surface Vehicle Mission

The mission is to start an ASV, a vehicle from DSOR, the MEDUSA, described in Appendix A, at position $[x, y, z] = [-2, 0.5, 0]\, m$ and then to make it follow its virtual target along a path similar to the one for the UAV, which is also a lawn mower, with a speed profile of $0.5\, m\, s^{-1}$. The selected gains for the control laws of the ASV from (4.18) and (4.24) are $K_P = 1$ for the surge speed and $K_P = 10$ for the yaw-rate, and also $K_I = 0.2$ for both laws. Figure 6.6 represents how the ASV follows the path as well as the virtual target, the green point, for each instant of time represented.

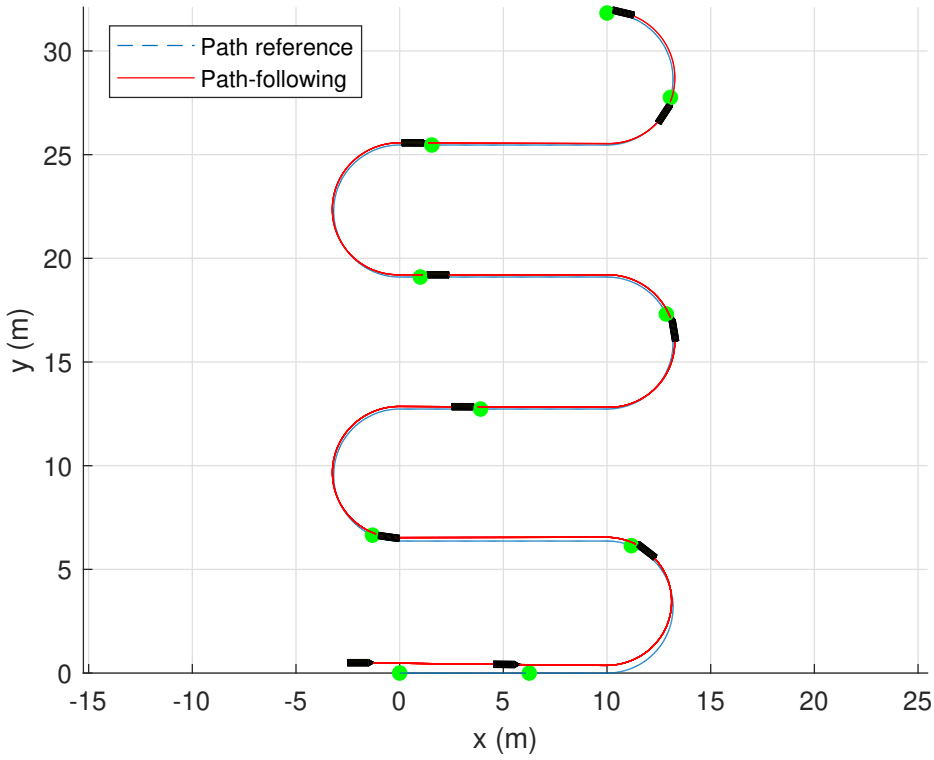

Figure 6.6: Single ASV Lawn-mowing Mission.

In the case of the ASV the value for distance between the vehicle and its virtual target from which the virtual target stops and waits is also set to 5 m. In figure 6.7 is also verified that the ASV can follow the intended path, the distance between the vehicle and its virtual target is kept below 25 cm.

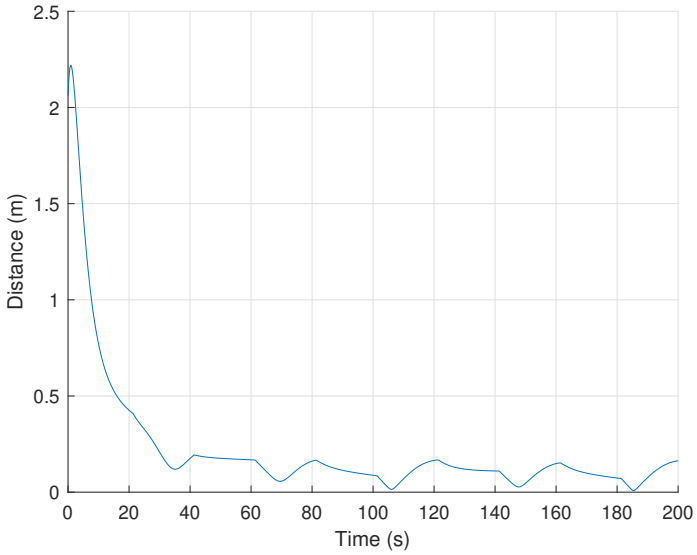

Figure 6.7: Single ASV Lawn-mowing Mission - distance to the virtual target along the mission.

The Surge speed and Yaw-rate controllers also seem to be able to track the proposed references as can be seen in 6.8.

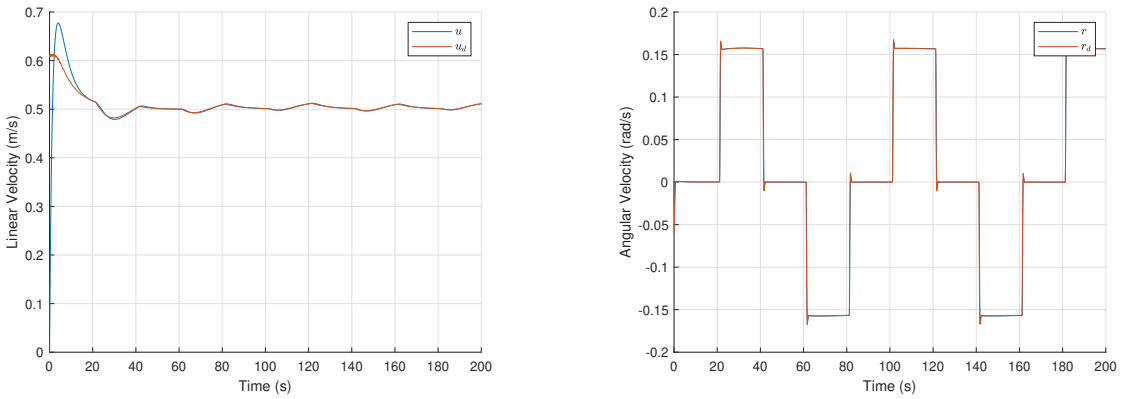

(a) Surge speed, u, reference tracking.

(b) Yaw-rate, r, reference tracking.

Figure 6.8: Single ASV Lawn-mowing Mission - reference tracking by the ASV controllers.

Regarding the PF algorithm it can be seen in figure 6.9 that $\dot{\gamma}$ converges to 1. It is also important to point out that the value for the distance between the vehicle and its virtual target from which the virtual target stops and waits is also set to 5 m. Similarly to the UAV the gain for the dynamic presented in (5.14) is $K_V = 1$.

Figure 6.10 presents the absolute value for the translational and rotational thrust, τ_u and τ_r, applied through the ASV thrusters.

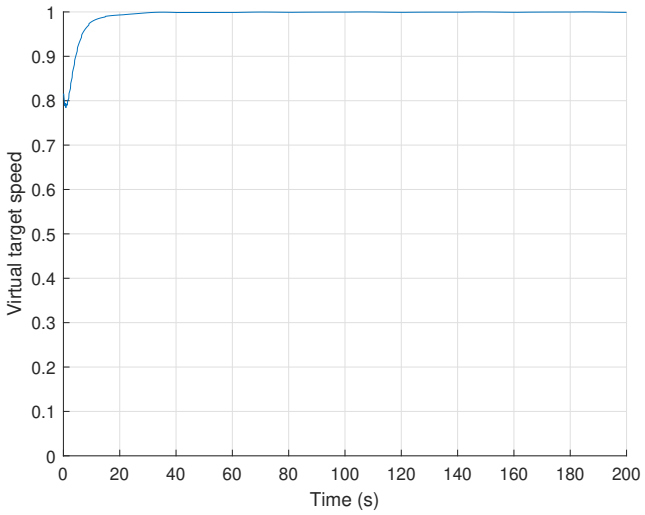

Figure 6.9: Single ASV Lawn-mowing Mission - virtual target speed $\dot{\gamma}$.

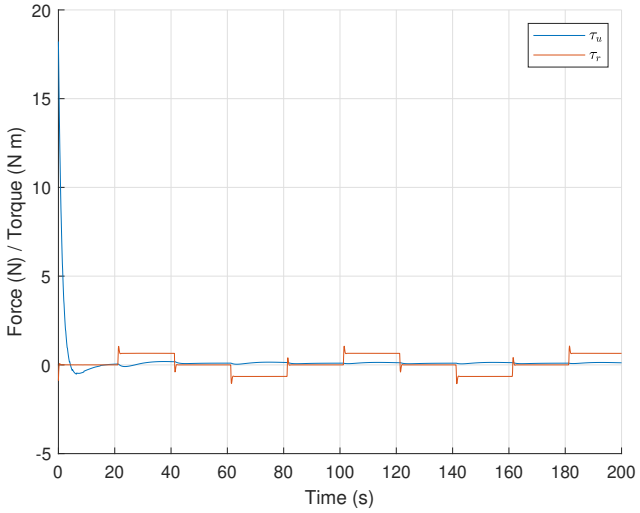

Figure 6.10: Single ASV Lawn-mowing Mission - translational and rotational thrust.

6.3 Cooperative Mission between an ASV and an UAV linked by a Tether

The cooperative mission is the combination of the previous individual missions, a lawn-mowing path with a relative shift of $[x, y, z] = [3, 3, 9]\, m$, which means that $\Delta z/\Delta x \approx 2.1213$, with both vehicles connected by a tether which is a considered disturbance on the UAV. There is a constant wind disturbance of $[-2, 0, 0]\, N$. To study the impact of sea ondulation it is added to the ASV an height periodic variation,

a sine wave with an amplitude of $20\,cm$ and a frequency of $0.2\,Hz$. Contrary to what happened in the previous sections, the noise is introduced in the positions of both vehicles to test the robustness of the entire system, it is gaussian noise with mean $0\,m$ and standard deviation of $0.25\,m$, $\mathcal{N}(0, 0.25)$. The vehicles also start in the same positions the UAV at $[x, y, z] = [1, 1, 2]$m and the ASV at $[x, y, z] = [-2, 0.5, 0]\,m$. The gains for the controllers of the vehicles are the same as the ones of the previous sections. The path for each vehicle is the same but now there is a continuous Cooperative Path-following (CPF) algorithm making both vehicles wait for each other while following their paths. The value selected for K and L from (5.22) are

$$K = \begin{bmatrix} 1 & 0 \\ 0 & 1 \end{bmatrix} \quad , \quad L = \begin{bmatrix} 1 & -1 \\ -1 & 1 \end{bmatrix}. \tag{6.1}$$

The threshold distance that defines whether the virtual target moves or not is kept at 5 m for both vehicles. Also, the gain for the dynamic presented in (5.14) is $K_V = 1$ for both vehicles. A representation of the cooperative mission in which both vehicles follow their path along with each other is illustrated in figure 6.11. It is also represented the virtual target, the green points, of each vehicle at each given instant of time.

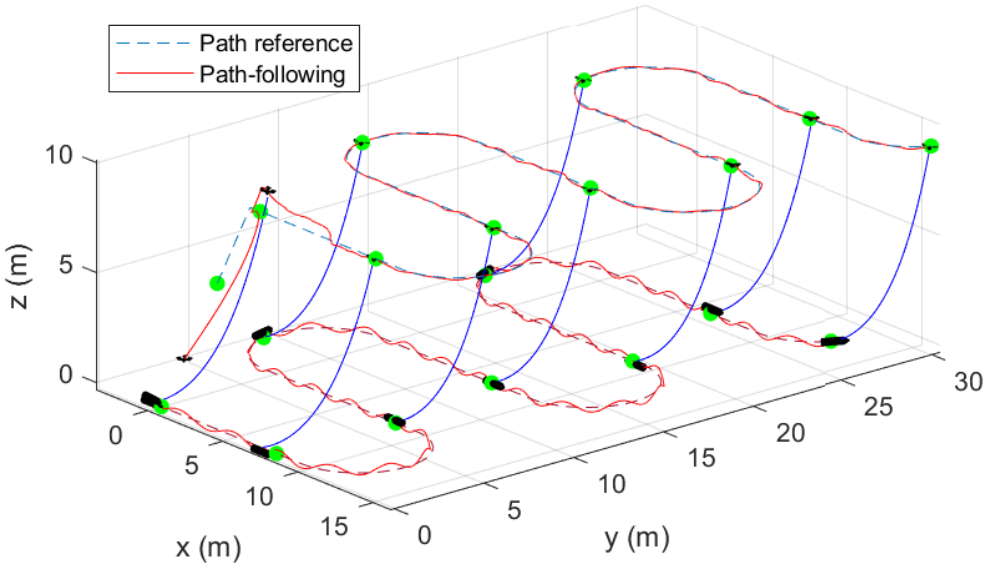

Figure 6.11: Cooperative Mission with tether.

In figure 6.12 is also verified that both vehicles follow the intended path, the distance between the UAV and its virtual target is kept below 25 cm as soon as it converges to the path, the distance between the ASV and its virtual target is also kept below 25 cm.

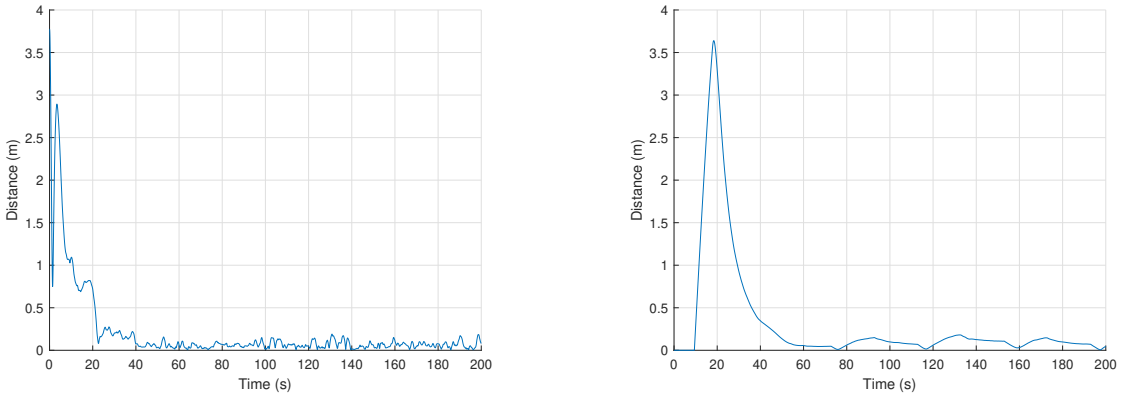

(a) UAV - distance to the virtual target.

(b) ASV - distance to the virtual target.

Figure 6.12: Cooperative Mission - distance to virtual target for each vehicle.

Regarding the PF algorithm it can be seen in figure 6.13 that firstly the marine vehicle does a slightly better job at following its path, then the other way around but ultimately their γ converge to the same value. In that same figure is also shown that $\dot{\gamma}_{uav}$ and $\dot{\gamma}_{asv}$ behave as expected by converging to 1, which means that both successfully converge to its own virtual target and are able to keep following it.

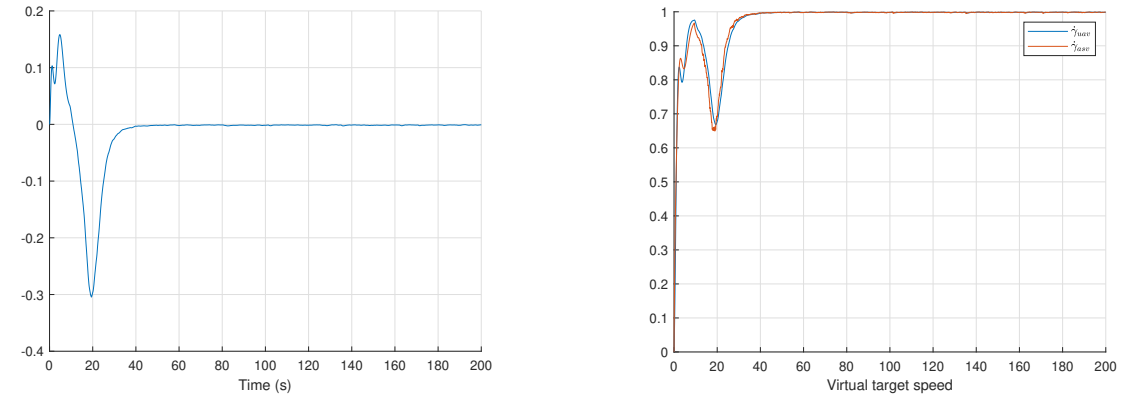

(a) Virtual target difference between vehicles - $(\gamma_{asv} - \gamma_{uav})$.

(b) Virtual target speed $\dot{\gamma}$ for each vehicle.

Figure 6.13: Cooperative Mission - virtual target parameter and speed $\dot{\gamma}$ behaviour for each vehicle.

This means that both vehicles converge to their virtual targets and their virtual targets are also following each other with similar values for γ. This can also be confirmed by figure 6.14 where it is

possible to observe how the CPF algorithm is correcting the values for $\dot{\gamma}$ for each vehicle in order to get values for γ that follow each other and ultimately get cooperation between vehicles. At first, the ASV virtual target has to slow down with respect to the UAV virtual target, due to the fact that is just waiting for the UAV to converge to its target while the ASV is already there. However, when the aerial vehicle starts the lawn-mowing it is corrected the other way around because the ASV from that point on has to converge to a moving target while the UAV was already in motion along with its target. Once both are in motion and coordinated the correction converges to zero which means that the CPF is working properly for similar paths and speed profiles.

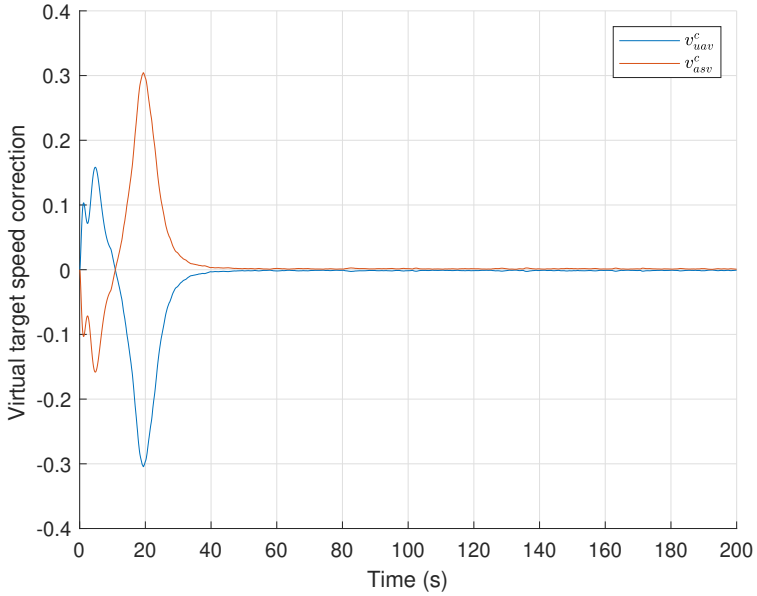

Figure 6.14: Cooperative Mission - Correction of the virtual target speed for each vehicle.

Finally, it is also important to state that the success of the PF for the UAV means that the tether and wind disturbance is being rejected by the integral part of its controller. The evolution of the absolute value of each force applied to the UAV, which are in this case: the gravitational force, a wind constant disturbance, the tether disturbance and the force to accelerate the vehicle, but also the thrust that the vehicle must generate to compensate the first and the second and still be able to move as intended is presented in figure 6.15(a). The torque applied by the tether on the aerial vehicle is considered in simulation however, due to the fact that its mounting point is considered at a $10\,cm$ distance in the z-axis , makes its effect as a rotational disturbance almost residual. The absolute value for the translational and rotational, τ_u and τ_r, thrust applied through the ASV thrusters is shown in figure 6.15(b).

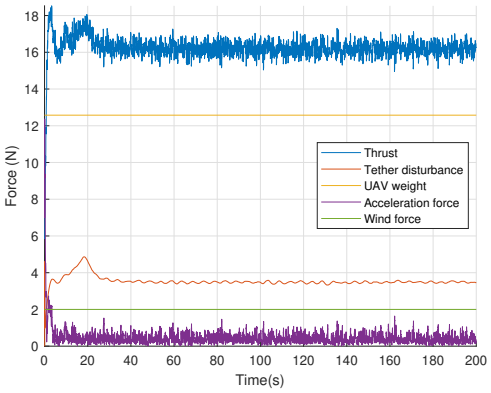

(a) Absolute value for the forces applied to the UAV.

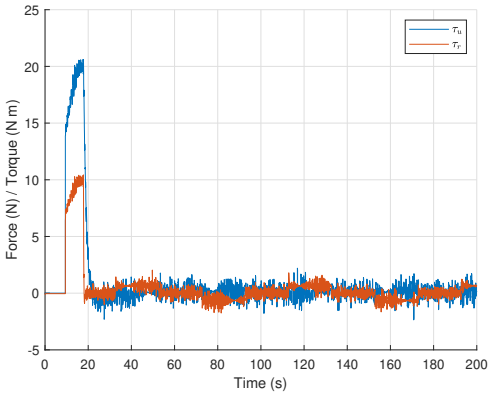

(b) Absolute value for the force and torque applied to the ASV.

Figure 6.15: Cooperative Mission - absolute value of the forces applied to the vehicles.

The tether length, as expected, increases while the UAV is on its way to the desired relative position and then when it gets there, it oscillates, due to the previously stated variation in the height of the ASV, around a value computed by (2.38) with an increasing tension from the slack length of 10%. Although if one wants to implement a pulley system capable to track a reference for the tether length its response would not be instantaneous, therefore for simulation it was introduced $\dot{L} = -K_T(L - L_{REF})$, which is a first-order system, to get a closer approximation of the behaviour of an actual pulley, where L_REF is the reference for the cable length given by the function defined in Chapter 2. Its departure angle is always kept above $0°$, which means that, in the worst case scenario, the ASV mounting point being at the water level, the tether does not touch the water. The evolution of the tether length and departure angle is shown in figure 6.16.

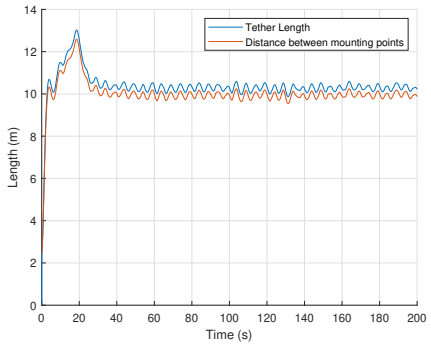

(a) Tether Length.

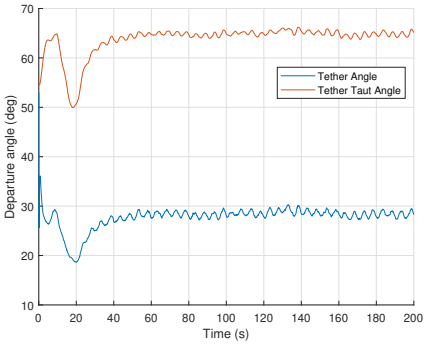

(b) Tether departure angle in ASV mounting point.

Figure 6.16: Cooperative Mission - tether length and departure angle.

6.4 ROS Simulation - a new Tether Plugin

As was stated before in Chapter 1 one of the main contributions of this work is a *Gazebo* Plugin to include the tether in simulation in a ROS environment. This environment was developed by the DSOR and further adapted to a similar scenario in [6]. It runs in *Ubuntu 20.04LTS* and with ROS Noetic [35]. To perform the simulations it was used *Gazebo* which is a three-dimensional (3D) simulator that runs a physics engine. Three plugins were used in this simulation, the UUVSimulator Plugin [36], the PX4 SITL Gazebo Plugin [37] and the tether Plugin. The UUVSimulator Plugin offers the possibility for the user to add new vehicles through Computer Aided Design (CAD) and even dynamics either for the thrusters or the actual vehicles. It also provides a virtual set of realistic sensors such as Attitude and Heading Reference System (AHRS), Differential Global Positioning System (DGPS) and Doppler Velocity Log (DVL), and also to simulate ocean currents. The DSOR used this plugin to model the MEDUSA vehicles, which are described in Appendix A and located in the farol_gazebo repository [38]. By introducing its dynamics and specifications along with a CAD model to accomplish virtual missions with it. A snapshot of the marine vehicle on a simulation is in figure 6.17.

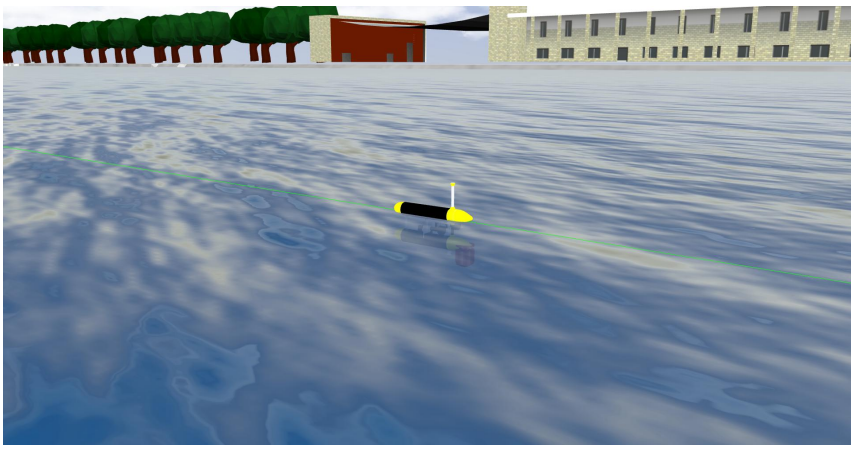

Figure 6.17: *Gazebo* Simulation - MEDUSA vehicle.

The PX4 SITL Gazebo Plugin allows to simulate with the 3D Robotics (3DR) Iris quadrotor, which is briefly described in Appendix B. This plugin is much more ready to go because contrary to what happened with the marine vehicles, which had to be introduced, these vehicles are very similar to those available in the Institute for Systems and Robotics (ISR), so it becomes viable to be used for simulation purposes. A snapshot of the aerial vehicle on a simulation is in figure 6.18.

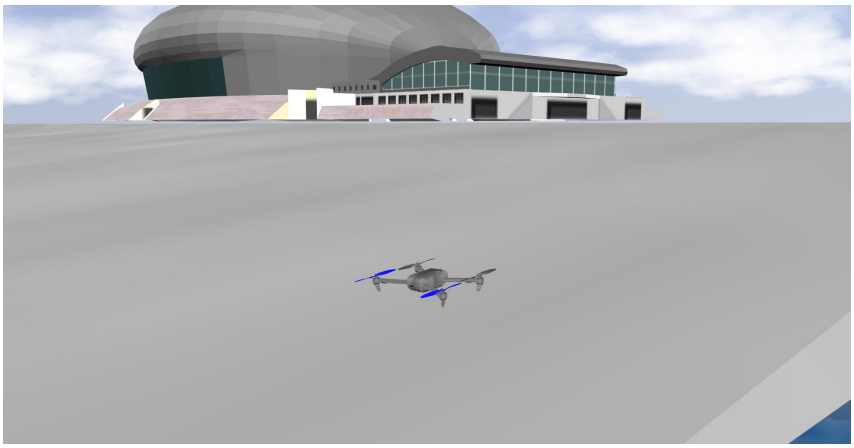

Figure 6.18: *Gazebo* Simulation - 3DR Iris vehicle.

The tether Plugin is a discretization of the equation (2.11) which gives the altitude of any point in a catenary given the horizontal span of that point from the ASV mounting point, the tether length, computed by the polynomial fit from (2.38) and the relative position between the two extremities of the cable. The tether is composed of a fixed number of joints and links, each joint is a point in the catenary which is connected by a straight link that dynamically stretches and shrinks to the distance between each of those joints through the whole simulation. The larger number of joints and links used the more realistic the simulation may look, however, it is important to clarify that each of these pairs is a body that the simulator has to render therefore the increase of bodies may overload the whole system. The plugin also computes and applies the force and torque which are being exerted on the UAV. The impact of the tether on the ASV is neglected because it is considered residual. The aerodynamic effects are also ignored. A snapshot of the tether on a simulation is in figure 6.19, each red dot is a joint and each yellow cylinder is a link.

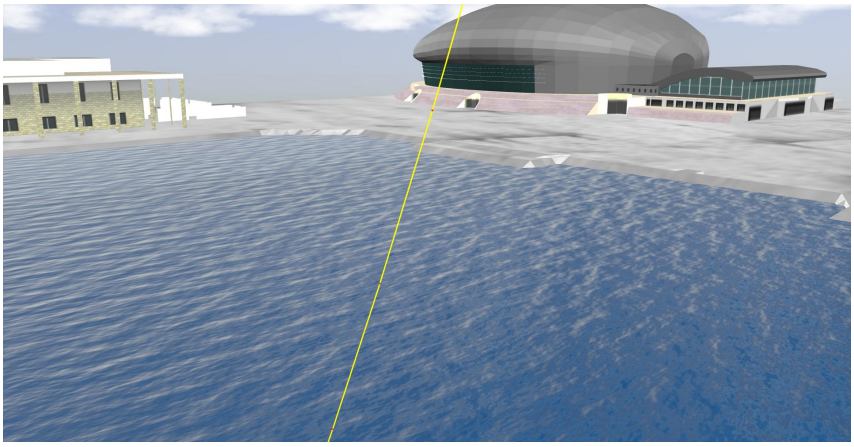

Figure 6.19: *Gazebo* Simulation - Tether.

The simulation world used is in a CAD representation of Doca dos Olivais in Lisbon, Portugal, which is where usually DSOR conducts real water experiments with the MEDUSA vehicles. This world is presented in figure 6.20.

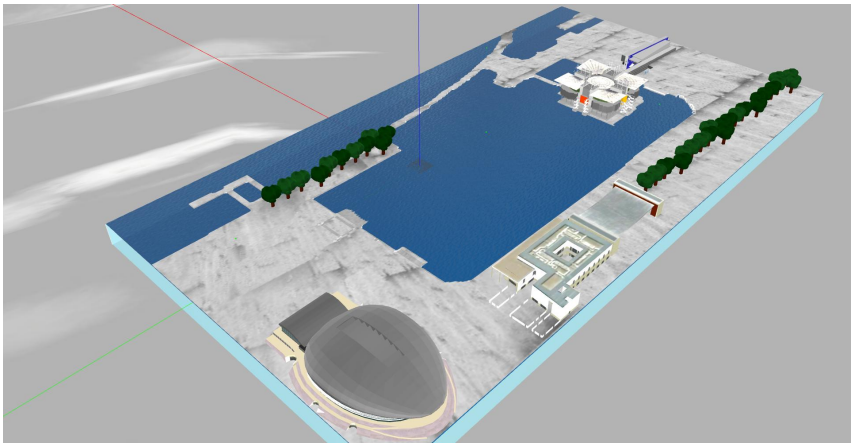

Figure 6.20: *Gazebo* Simulation - 3D world, Doca dos Olivais, Lisboa, Portugal.

The full system, which is the two vehicles attached by the tether is presented in figure 6.21. The mounting points of the tether are virtually above and below the ASV and UAV respectively.

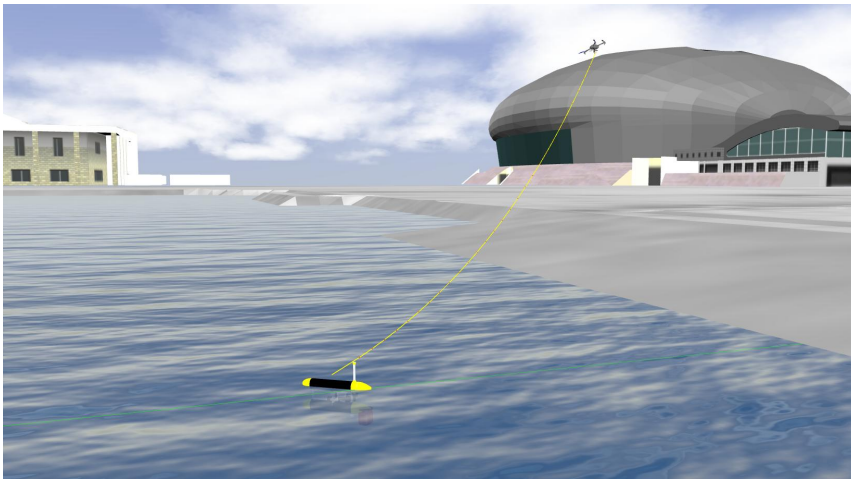

Figure 6.21: *Gazebo* Simulation - full system the UAV, ASV and the tether.

The goal of this section is to demonstrate some of the features of the tether plugin. To do so it was simulated in this environment a generic lawn mowing type of mission with a fixed relative position between vehicles. Therefore the focus is how the tether behaves, which is the novelty, rather than the behaviour of the actual vehicles or even the success of the CPF. Despite all this, results will be presented below regarding the cable in the context of a successful mission. The simulation architecture is presented in figure 6.22. Both vehicles have four nodes running the Path Manager node which is

responsible to feed the PF node given a path and its parameter, the PF node includes the laws that allow each vehicle to follow its target, its velocity it is corrected in the CPF node which is always communicating with the Network Manager node which in turn communicates with the local network the state of the virtual target via a discrete protocol, an Event-Triggered Communications (ETC) strategy. The discrete scheme for communication would not be the best choice because there is a tether that guarantees a wired continuous line of communication, however since the main focus is the tether this was kept as it was. The actual vehicle controllers and estimation filters are secured by the PX4 autopilot that is linked to the previously mentioned nodes via MAVLink protocol [39] for the UAV. For the MEDUSA vehicle, two separate ROS nodes are used both for the Inner-loop controllers and for the Kalman filter which communicates with *Gazebo*.

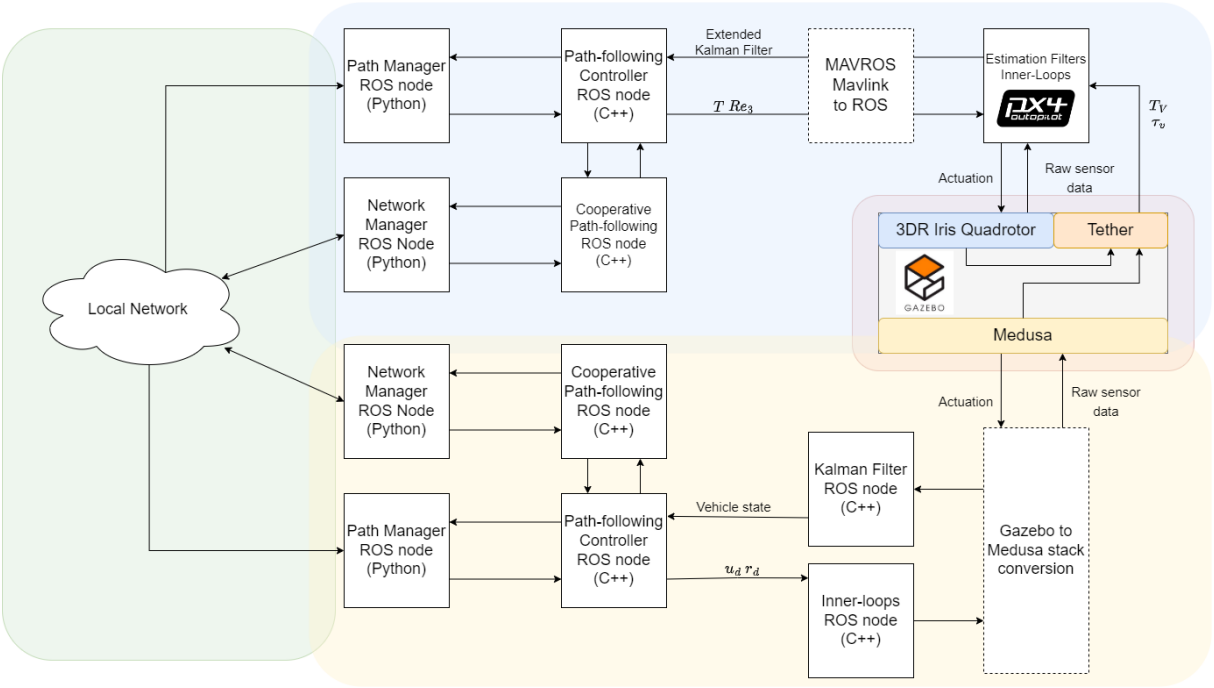

Figure 6.22: *Gazebo* Simulation - simulation architecture.

The mission in study is represented with an aerial two-dimensional (2D) view in figure 6.23. The vehicles have a predefined path shift of $[x, y, z] = [3, 3, 5]\,m$, which means that $\Delta z/\Delta x \approx 1.1785$. This does not mean that the vehicles have always this relative position and this will be clearer in the following figures. The formation speed is $0.5\,m\,s^{-1}$. At the start, the UAV is further from the target but it gets there quicker than the ASV, which means that it has to wait for the marine vehicle to also get to its target to only then start their cooperative mission. The UAV, the Iris quadrotor, and its path are represented by the black figure and the orange line. The ASV, the MEDUSA, and its path are represented by the yellow figure and line.

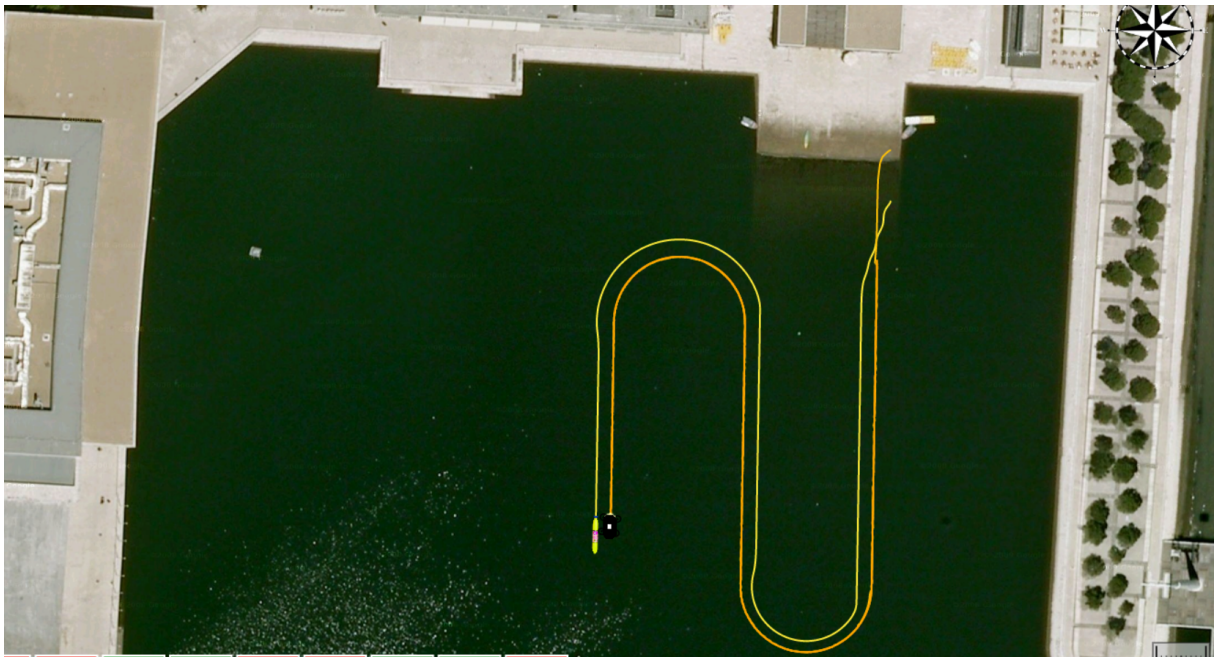

Figure 6.23: *Gazebo* Simulation - vehicle paths.

The tether departure angle at the ASV mounting point is kept as a positive angle, which is shown in figure 6.24(a). This confirms the success of the tether length management, which is also illustrated in 6.24(b), and that it never touches the water. There is a moment that is relevant to draw attention which occurs around the instant $t = 250\,s$ where the tether length is reduced around $1\,m$, this section of time is directly related to the first arc of circumference where the vehicles are closer than at any other time in the mission.

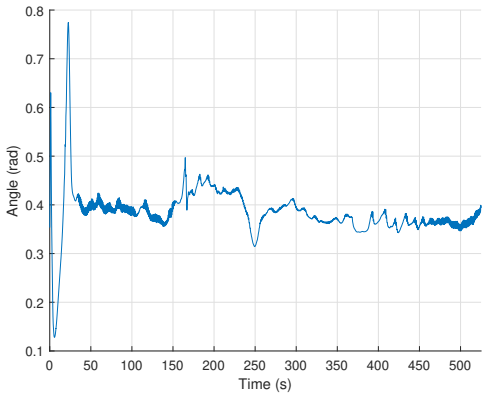

(a) Tether departure angle at the ASV mounting point.

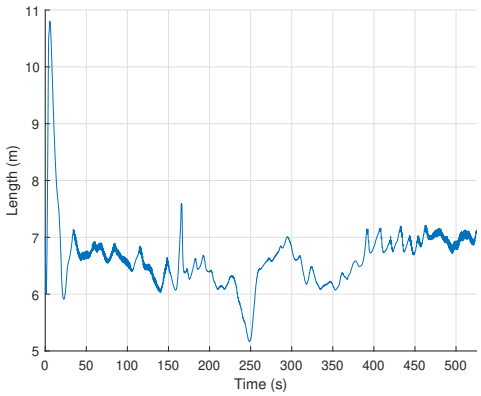

(b) Tether Length.

Figure 6.24: *Gazebo* Simulation - tether length and departure angle.

The magnitude of the disturbance exerted by the cable on the UAV through the whole path is described in figure 6.25. The first peak, where it reaches around $5\,N$, happens due to the fact that when the UAV converges to its virtual target the vehicles relative position increases and then decreased until the ASV also did. This led to a bigger tether length and therefore to a bigger disturbance. When both started the cooperation it stabilized below $2.5\,N$ which is a reasonable magnitude for a system with all the previously stated features.

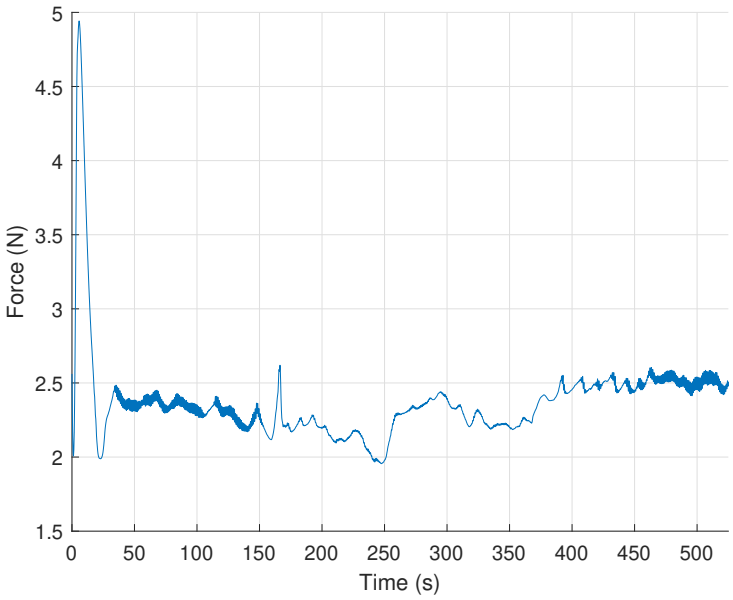

Figure 6.25: *Gazebo* Simulation - tether disturbance.

7

Conclusion and Future Work

Contents

7.1 Conclusion

This dissertation seeks to include a tethered connection between an aerial vehicle and a marine vehicle through a cooperative mission. This has the advantage of allowing the installation of a larger battery for the aerial vehicle on the surface vehicle where weight is a much lesser issue. This new power supply approach also brings the possibility for vehicles to be able to transmit data continuously, which includes the necessary communications for cooperation, and in addition, allows to significantly increase the flight time of the Unmanned Aerial Vehicle (UAV). The usage of a cable linking the vehicles creates some problems, one of which is addressed in this work which is tether length management. The idea was to have the cable in a state between taut, which can impair the performance of the aerial vehicle, and slack to the point of touching the water. The cable must have a positive departure angle at the Autonomous Surface Vehicle (ASV) having some slack in relation to the scenario in which it is fully stretched.

In Chapter 2 this problem is addressed by first modelling the cable as a catenary and then creating a polynomial approximation for the desired length for a given relative position between vehicles this proved to be a good approach and revealed that certain relative positions are better than others, which means that have bigger margins in terms of tolerance both for possible errors in a mission context or even for possible sea ripples.

In Chapters 3 and 4 it was defined the notation and the modelling of each type of vehicle and then two control strategies were specified. For the UAV it was developed an inner-loop outer-loop strategy, the inner part was meant to follow orientation references while the outer part was to track position, linear velocity and acceleration. For the ASV it was used two inner-loops to track references for the surge speed and the yaw rate.

Chapter 5 starts by outlining the individual Path-following (PF) strategy for each vehicle by designating a virtual entity to be followed, this target moves along the path with a velocity that depends on the distance to its respective vehicle, if the vehicle is close the target moves at the intended speed profile for the path this velocity decreases with increasing distance until a point, which is previously defined, where the target simply stops waiting for a new approach of the vehicle. Then the cooperation was specified as a correction of the virtual targets' speed to get the targets synchronized in each of their paths.

Lastly, in Chapter 6 the results are demonstrated with regard to a generic lawn-mowing path. At first, it is analysed individually for each vehicle its capability to follow a path, then both are joined and connected by a tether into a similar mission to analyse the Cooperative Path-following (CPF) performance but also the tether management success. All of these were conducted in a *MATLAB* environment. The system overall behaved as desired for this specific system when working in a well-chosen working zone. The Chapter ends with the presentation of a new tether plugin for *Gazebo*. This plug-in was coupled to a formation of two vehicles, the MEDUSA and the 3D Robotics (3DR) Iris, in a lawn-mower path to observe if it behaved as desired. As expected it did, especially when in a reasonable working zone.

7.2 Future Work

The work developed for this master's dissertation can pave the way for new research and developments regarding this topic. Some issues were left unexplored and most likely others could be improved and even implemented. Some of those topics are listed below.

- Implementation of the pulley capable of tracking a reference for the tether length based on the polynomial fit developed in (2.38).
- To study the tethers available and which ones would fit such missions, to do not treat this cable only as a theoretical entity.
- To develop a tether plug-in to include a more complex model for the tether, including aerodynamic effects and others, with the ultimate goal to make it as realistic as possible.
- To specify and study the mechanisms related to the take-off, and landing of the UAV as well as safety measures regarding any undesired and possibly harmful actions by any intervening part of the system.
- To migrate the system to a more constrained environment, for example with some obstacles to avoid.

Bibliography

[1] R. W. Beard and T. W. McLain, *Small Unmanned Aircraft, Theory and Practice*, 2012.

[2] L. Zikou, C. Papachristos, and A. Tzes, "The power–over–tether system for powering small uavs: Tethering–line tension control synthesis," *23rd Mediterranean Conference on Control and Automation (MED)*, June 2015.

[3] K. A. Talke, "Hanging tether management for unmanned air-surface vehicle teams," Ph.D. dissertation, UC San Diego, 2021.

[4] J. Ribeiro, "Motion control of single and multiple autonomous marine vehicles," Master's thesis, Instituto Superior Técnico, October 2011.

[5] MEDUSA — DSOR. [Online]. Available: http://dsor.isr.ist.utl.pt/vehicles/medusa/

[6] M. Jacinto, "Cooperative motion control of aerial and marine vehicles for environmental applications," Master's thesis, Instituto Superior Técnico, December 2021.

[7] APMCOPTER — Iris - The Ready to Fly UAV Quadcopter. [Online]. Available: https://www.arducopter.co.uk/iris-quadcopter-uav.html

[8] Elistair. [Online]. Available: https://elistair.com/

[9] Hoverfly. [Online]. Available: https://hoverflytech.com/

[10] ViperDrones. [Online]. Available: https://viper-drones.com/systems/tethered-systems/

[11] L. Lapierre, D. Soetanto, and A. Pascoal, "Nonsingular path following control of a unicycle in the presence of parametric modelling uncertainties," *International Journal of Robust and Nonlinear Control*, vol. 16, pp. 485–503, July 2006.

[12] A. P. Aguiar and J. P. Hespanha, "Trajectory-tracking and path-following of underactuated autonomous vehicles with parametric modeling uncertainty," *IEEE Transactions on Automatic Control*, vol. 52, no. 8, pp. 1362–1379, August 2007.

[13] B. Rubí, R. Pérez, and B. Morcego, "A survey of path following control strategies for uavs focused on quadrotors," *Journal of Intelligent and Robotic Systems: Theory and Applications*, vol. 98, pp. 241–265, May 2020.

[14] T. I. Fossen, M. Breivik, and R. Skjetne, "Line-of-sight path following of underactuated marine craft," vol. 36. IFAC Secretariat, 2003, pp. 211–216.

[15] F. Vanni, A. P. Aguiar, and A. M. Pascoal, "Cooperative path-following of underactuated autonomous marine vehicles with logic-based communication," *IFAC Proceedings Volumes*, vol. 41, pp. 107–112, 2008.

[16] A. P. Aguiar and A. M. Pascoal, "Coordinated path-following control for nonlinear systems with logic-based communication," *Proceedings of the 46th IEEE Conference on Decision and Control*, December 2007.

[17] R. Ghabcheloo, A. P. Aguiar, A. Pascoal, C. Silvestre, I. Kaminer, and J. Hespanha, "Coordinated path-following in the presence of communication losses and time delays," *SIAM Journal on Control and Optimization*, vol. 48, pp. 234–265, 2009.

[18] N. T. Hung, A. M. Pascoal, and T. A. Johansen, "Cooperative path following of constrained autonomous vehicles with model predictive control and event-triggered communications," *International Journal of Robust and Nonlinear Control*, vol. 30, pp. 2644–2670, May 2020.

[19] N. T. Hung and A. M. Pascoal, "Consensus/synchronisation of networked nonlinear multiple agent systems with event-triggered communications," *International Journal of Control*, pp. 1–10, 2020.

[20] R. Olfati-Saber, J. A. Fax, and R. M. Murray, "Consensus and cooperation in networked multi-agent systems," *Proceedings of the IEEE*, vol. 95, pp. 215–233, January 2007.

[21] W. Ren and E. Atkins, "Distributed multi-vehicle coordinated control via local information exchange," *International Journal of Robust and Nonlinear Control*, vol. 17, pp. 1002–1033, July 2007.

[22] J. Han, "From pid to active disturbance rejection control," *IEEE Transactions on Industrial Electronics*, vol. 56, pp. 900–906, February 2009.

[23] D. Cabecinhas, R. Cunha, and C. Silvestre, "A nonlinear quadrotor trajectory tracking controller with disturbance rejection," *Control Engineering Practice*, vol. 26, pp. 1–10, 2014.

[24] M. Tognon and A. Franchi, "Position tracking control for an aerial robot passively tethered to an independently moving platform," *20th IFAC World Congress*, 2017.

[25] D. Cabecinhas, R. Cunha, and C. Silvestre, "A trajectory tracking control law for a quadrotor with slung load," *Automatica*, vol. 106, pp. 384–389, August 2019.

[26] G. Yu, D. Cabecinhas, R. Cunha, and C. Silvestre, “Nonlinear backstepping control of a quadrotor-slung load system,” *IEEE/ASME Transactions on Mechatronics*, vol. 24, pp. 2304–2315, October 2019.

[27] R. M. P. P. de Matos Martins, “Flight control and position estimation for a tethered micro aerial robot,” *Instituto Superior Técnico*, December 2019.

[28] P. G. Ioppo, “The design, modelling and control of an autonomous tethered multirotor uav,” Master’s thesis, University of Stellenbosch, March 2017.

[29] K. A. Talke, M. de Oliveira, and T. Bewley, “Catenary tether shape analysis for a uav - usv team,” *2018 IEEE RSJ International Conference on Intelligent Robots and Systems (IROS)*, October 2018.

[30] R. M. Murray, Z. Li, and S. S. Sastry, *A Mathematical Introduction to Robotic Manipulation*, 1994.

[31] D. Mellinger and V. Kumar, “Minimum snap trajectory generation and control for quadrotors,” *2011 IEEE International Conference on Robotics and Automation*, May 2011.

[32] T. I. Fossen, *Handbook of marine craft hydrodynamics and motion control*. Wiley, 2011.

[33] A. P. Aguiar and A. M. Pascoal, “Modeling and control of an autonomous underwater shuttle for the transport of benthic laboratories,” 1997.

[34] ——, “Dynamic positioning and way-point tracking of underactuated auvs in the presence of ocean currents,” *41st IEEE Conference on Decision and Control*, December 2002.

[35] ROS Noetic. [Online]. Available: https://www.ros.org/

[36] M. M. M. Manhães, S. A. Scherer, M. Voss, and L. R. Douat, “Uuv simulator: A gazebo-based package for underwater intervention and multi-robot simulation.” IEEE, 2016.

[37] PX4 Autopilot User Guide. [Online]. Available: https://docs.px4.io/main/en/

[38] Farol Gazebo Repository in Github, Dynamical Systems and Ocean Robotics Laboratory (DSOR) in Institute for Systems and Robotics (ISR). [Online]. Available: https://github.com/dsor-isr/farol_gazebo

[39] MAVLINK. [Online]. Available: https://mavlink.io/en/

A

MEDUSA - marine vehicle description

This appendix turns to [4] and [6] to briefly describe the autonomous semi-submersible robotic vehicles, known as MEDUSA, which were created at the Laboratory for Robotics and Engineering Systems (LARSyS)/ISR. Each MEDUSA-class vehicle weighs around 30 kg and is made up of two 0.15 m $\times$ 1.035 m (diameter x length) acrylic housing tubes with aluminum end caps that are connected by an aluminum frame in the middle. The two bodies are separated by 0.15 meters. The bottom underwater tube houses the thruster electronics, an underwater camera, an acoustic modem (Tritech UK), and various small sensors, along with two packs of 7-cell lithium polymer batteries. The main computer unit (Epic computer NANO PV D5251, with an Intel Atom D525 dual-core processor, low power, 1.8GHz with 2GB RAM) is located in the upper body, which is partially above the water. It also houses navigation sensors (an attitude sensor - VECTORNAV VN-100) and a Global Positioning System (GPS) (GPS - Ashtech MB100). Two stern thrusters (SEABOTIX HPDC1507 Brushless thrusters) attached to the main frame directly control the yaw and surge motions. The vehicles have a 12-hour autonomy at the nominal speed of 1.0 m/s and may travel at a maximum speed of 1.5 m/s. Wi-Fi is used for inter-vehicle communications between various airborne or surface vehicles, and an underwater acoustic modem network can also be used.

In figure A.1 there is a representation of the MEDUSA and its size.

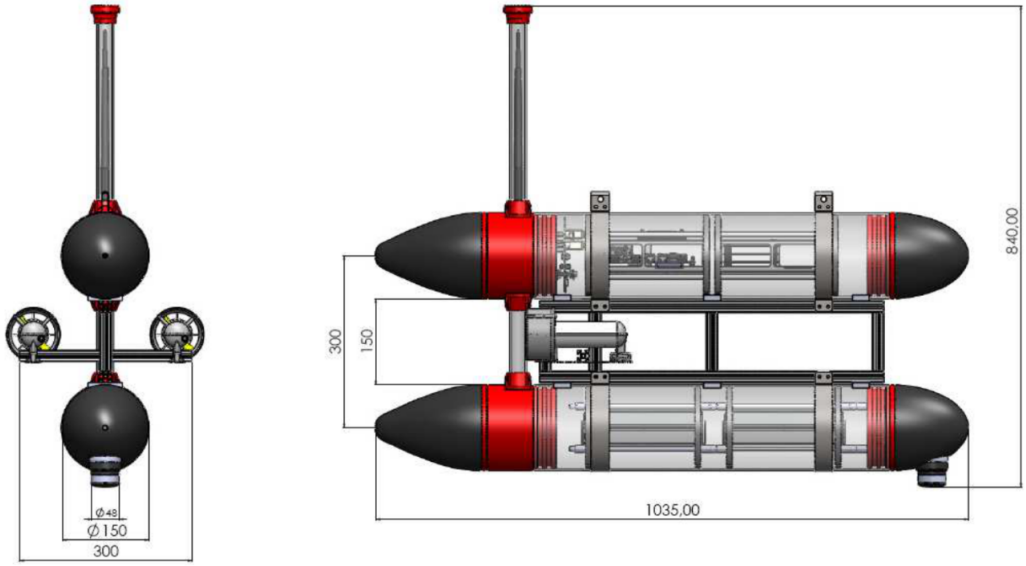

Figure A.1: Medusa vehicle representation (from [5]).

The model parameters for these type of marine vehicles are the ones presented in table A.1.

$X_{\dot{u}}$	$-20\,kg$	$Y_{\dot{v}}$	$-30\,kg$	$N_{\dot{r}}$	$-0.5\,kg\,m^2$
X_u	$-0.2\,kg\,s^{-1}$	Y_v	$-55.1\,kg\,s^{-1}$	N_r	$-4.14\,kg\,m\,s^{-1}$
$X_{\|u\|u}$	$-25\,kg\,s^{-1}$	$Y_{\|v\|v}$	$0.01\,kg\,m^{-1}$	$N_{\|r\|r}$	$-6.23\,kg\,m$

Table A.1: Medusa vehicle model parameters.

The vehicle has $m = 30kg$ and its moment of inertia about the z-axis is around $I_z = 1Kgm^2$. The thrusters can be used in common and differential mode to control the force for surge τ_u and the torque for the yaw motion τ_r which can be defined as

$$\tau_u = F_s + F_p, \tag{A.1}$$

$$\tau_r = l(F_s - F_p), \tag{A.2}$$

where F_s is the starboard relative force, F_p is the same but for the port and $l = 0.15m$ is the length of the component that connects the thruster to the vessel. There is a thrust curve for each thruster which is

$$F(F_{in}) = a|F_{in}|F_{in}, \tag{A.3}$$

in which $a = 0.0036$ and $F_{in} \in [-100, 100]$ that is normalised and then used by the motor allocation

driver. In [6] it is also presented a model for the thrusters experimentally created in the ISR test tank in Taguspark campus of Instituto Superior Técnico (IST) which is defined by the block diagram of figure A.2 including a first order system

$$G(s) = \frac{K_0}{s + K_0} e^{-s\tau}, \tag{A.4}$$

with $K_0 = 7.2115$ and $\tau = 0.346s$.

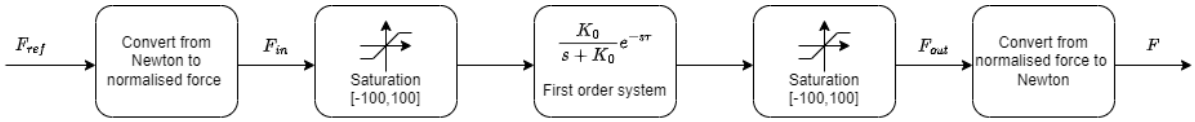

Figure A.2: Block diagram for the thruster model (adopted from [6]).

B

3DR Iris Quadrotor - aerial vehicle description

This appendix turns to [6] and [7] to briefly describe the Iris quadrotor, which was utilized for simulation, is introduced in this appendix. Figure B.1 depicts the 3DR Iris quadrotor, a commercial vehicle created and produced by 3DR. It has a motor to motor dimension of $550mm$ and a height of $100mm$, it weighs roughly $1.282kg$ with battery. Its payload capacity is $400g$. It has an average flight time of 10-15 minutes. Its CAD model is open source, and the PX4 SITL Plugin [37] offers a gazebo simulation model. The UAV features four rotors and with an X-shaped frame. Several sensors, including a barometer, magnetometer, Inertial Measurement Unit (IMU), and Differential Global Positioning System (DGPS), are integrated inside its casing. Its moments of inertia are $Ix = 0.029kg\ m^2$, $Iy = 0.029kg\ m^2$, and $Iz = 0.055kg\ m^2$. The vehicle total thrust curve may be defined as a quadratic function

$$T(T_{in}) = aT_{in}^2 + bT_{in}, \tag{B.1}$$

with $a = 34$ and $b = 7.2$, with $T_{in} \in [0, 1]$ which is the normalised input used by the quadrotor motor mixer.

Figure B.1: 3DR Iris vehicle representation (from [7]).